Origin, Bulk Chemical Composition and Physical Structure of the Galilean Satellites of Jupiter: A Post-Galileo Analysis

A.J.R. Prentice *

Department of Mathematics and Statistics,

Monash University

Clayton, Victoria 3168

AUSTRALIA

and

Jet Propulsion Laboratory

California Institute of Technology

Pasadena, California, USA

Submitted to *Earth, Moon, and Planets*

May 1999

*E-mail: AJRP@vaxc.cc.monash.edu.au

Abstract

The origin of Jupiter and the Galilean satellite system is examined in the light of the new data that has been obtained by the NASA Galileo Project. In particular, special attention is given to a theory of satellite origin which was put forward at the start of the Galileo Mission and on the basis of which several predictions have now been proven successful (Prentice, 1996a, b, c). These predictions concern the chemical composition of Jupiter's atmosphere and the physical structure of the satellites.

origin of the solar system

According to the proposed theory of satellite origin, each of the Galilean satellites formed by chemical condensation and gravitational accumulation of solid grains within a concentric family of orbiting gas rings. These rings were cast off equatorially by the rotating proto-Jovian cloud (PJC) which contracted gravitationally to form Jupiter some 4 ½ billion years ago. The PJC formed from the gas and grains left over from the gas ring that had been shed at Jupiter's orbit by the contracting proto-solar cloud (PSC). It is claimed that turbulent stress arising from supersonic convective motions within both the PJC and PSC provided the means for the disposal of excess spin angular momentum in discrete gas rings.

The temperatures T_n of the system of gas rings shed by the PSC and PJC vary with their respective mean orbital radii R_n ($n = 0,1,2,\ldots$) according as $T_n \propto R_n^{-0.9}$. If the planet Mercury condenses at 1640 K, so accounting for the high density of that planet via a process of chemical fractionation between iron and silicates (Lewis, 1972; Prentice, 1990,

1991), then T_n for the proto-solar gas ring at Jupiter's orbit is 158 K. As this is just 5 K less than the local condensation temperature of water ice, only 35% of the water vapour can condense. Thus fractionation between rock and ice, together with a natural enhancement in the abundance of solids relative to gas which takes place through gravitational sedimentation of solids onto the mean orbit of the gas ring, ensures that if the rock abundances in the PJC are enhanced by a factor of 2 relative to solar values then H_2O is enhanced only by a factor of 1.3. This accounts for the nearly equal proportions of rock and ice in each of Ganymede and Callisto.

At the orbits of Io and Europa the condensate consists solely of hydrated rock (h-rock). For Ganymede the condensate consists of h-rock and H_2O ice in the mass percents 52.5 : 47.5. For Callisto, NH_3 ice makes up ~5% of the condensate mass next to h-rock (~50%) and H_2O ice (~45%). $Mg(OH)_2$ and SiO_2 are the chief repositories of Mg and Si in Europa, Ganymede and Callisto h-rock. FeS is the most copious iron mineral at all four satellite orbits. The remaining iron condenses as pure Fe and Fe_2SiO_4 at the orbit of Io and as Fe_3O_4 for the others.

Detailed thermal and structural models for each of Europa, Ganymede and Callisto are constructed on the basis of the above initial bulk chemical compositions. For Europa (E), a predicted 2–zone model consisting of a dehydrated rock core of mass 0.912 M_E and a 150 km thick *frozen* mantle of salty H_2O yields a moment-of-inertia coefficient which matches the Galileo Orbiter gravity measurement (Anderson *et al.*, 1997a, 1998a). For

Ganymede (G), a 3–zone model possessing an inner core of solid FeS and mass ~0.116 M_G and an outer H_2O ice mantle of mass ~0.502 M_G is needed to explain the Galileo gravity data. Ganymede's native magnetic field was formed by thermoremanent magnetization of Fe_3O_4 within a ~65 km thick rocky layer located about 1450 km from the satellite centre. Lastly, a predicted cold, chemically-uniform and magnetically inert model for Callisto was confirmed by the initial Galileo data (Prentice, 1996a, 1996c). A new Callisto (C) model is proposed consisting of a core of mass 0.826 M_C containing a uniform mixture of h-rock (60% by mass) and H_2O and NH_3 ices, and capped by mantle of ice. If the ice cap formed by accretional melting of H_2O and NH_3 and the NH_3 refroze as $NH_3 \cdot 2H_2O$ (including dissolved NaCl), the low melting temperature ~176 K of this ice may yield a thin, present-day, electrically conducting liquid layer at the core boundary, in line with the Galileo magnetometer observations (Khurana *et al.*, 1998).

1. Introduction

The successful completion of the Galileo spacecraft primary mission to Jupiter in December 1997, has brought a wealth of new information about this planet, its magnetosphere, and its family of four large Galilean satellites. Whilst the Galileo data has consolidated some of our previous ideas about the makeup of the Jovian system, especially those which have been acquired since the Voyager 1 and 2 missions in 1979, there have also been many new discoveries that were completely unforeseen. For example, the finding by the Galileo Probe (Niemann *et al.*, 1996) that the Jovian atmosphere is very dry, at least in the region where the Probe entered, was not predicted

by any theory. Nor was the discovery of Ganymede's native magnetic field, whose strength is an order of magnitude larger than the local ambient field (Kivelson *et al.*, 1996). The fact that this moon is so strongly differentiated in its internal structure compared to its nearby twin Callisto (Anderson *et al.*, 1996a, 1997b, 1998b) presents us with a deepening theoretical mystery (Mueller and McKinnon, 1988; McKinnon, 1997). Callisto has no native magnetic field and appears thermally dormant. Why are Ganymede and Callisto so different?

With regard to Io, it now seems certain that this moon contains a partly molten interior (Anderson *et al.*, 1996b), as first predicted by Peale *et al.* (1979). But the extent of the melted region and its precise chemical composition are unknown. FeS is mostly likely the chief melt constituent (Prentice and ter Haar, 1979; Prentice, 1996b). And lastly, the discovery of the disrupted ice crust of Europa means that throughout some portion of this moon's past, it has been surrounded by a warm ocean some 100–200 km deep (Anderson *et al.,* 1997a; Carr *et al.*, 1998). Such an ocean may have formed through dehydration of an initial, heavily-hydrated, rocky interior (Prentice and ter Haar, 1979; Ransford *et al.*, 1981).

This paper explores the origin, bulk chemical composition and physical structure of the Galilean satellite system of Jupiter in the light of the Galileo spacecraft data. It is the sequel to a pre-Galileo analysis of Jupiter's formation (Prentice, 1996a). Several important predictions which were put forward then have now been tested by the Galileo data. Both then and now it is assumed that the Galilean satellite system is a miniature

version of the sun's planetary system and that both systems were formed by similar mechanisms. In particular, the Galilean satellites, like solid planetary cores, formed through the chemical condensation and gravitational accumulation of myriads of grains within a concentric family of orbiting gas rings. These had been cast of close to the present mean orbital positions by the primitive cloud of gas and dust which contracted gravitationally to form Jupiter. This modern version of Laplace's nebular hypothesis of solar system origin is discussed in Section 2 below.

In Sections 3 and 4, the gravitational contraction of the proto-solar cloud is examined in order to estimate the physical and chemical properties of the gas ring from which Jupiter's embryonic planetary core and primitive atmosphere formed. The gravitational contraction of the proto-Jovian cloud is explored in Section 5, enabling a determination of the properties of the gas rings from which the Galilean satellites condensed. The initial chemical composition of each of the Galilean satellites is calculated in Section 6. These compositions form the basis for the construction of detailed thermal and structural models of the satellites. Section 7 describes the computational codes which generate the satellite models. Section 8 presents the results of the numerical calculations along with a careful comparison of these results against the Galileo Orbiter observations. The conclusions of this study are given in Section 9.

2. Main features of the modern Laplacian theory

According to the Laplace (1796) nebula hypothesis of solar system origin, which is depicted in Figure 1, the planets accreted close to their present orbital positions from rings of gas that had been shed by the primitive contracting solar cloud. These rings were cast off by this cloud from its equatorial zone as a means for disposing of excess spin angular momentum during its inward radial contraction, starting from the orbit of Neptune. Of course, Laplace did not specify the physical mechanism for shedding discrete gas rings and the hypothesis was eventually abandoned since, more seriously, it could not reconcile the very small mass of the planetary system relative to the sun's mass. That is, the process of ridding angular momentum must also lead to a substantive loss of mass from the cloud. This lost mass should now be shared amongst the planets.

In 1928, Jeans noted that if the proto-solar cloud was very centrally condensed, i.e., possessed a very small axial moment-of-inertia factor $f << 1$, and if it rotated uniformly like a solid body then it could dispose of all of its excess spin momentum at the expense of losing little mass. That is, as Schatzmann (1949) demonstrated, if $L(R_e)$ and $M(R_e)$ denote the residual angular momentum and mass of the cloud at equatorial radius R_e, then these quantities scale as

$$L(R_e) = L(R_0)[R_e/R_0]^{1/(2-3f)}$$
$$M(R_e) = M(R_0)[R_e/R_0]^{f/(2-3f)} \qquad (1)$$

Here R_0 denotes Neptune's mean orbital radius. The problem, therefore, is to find a mechanism that may lead to a low value for f and ensure uniform rotation. In addition, the mechanism should explain why the material is shed discretely, as individual gas rings, rather than as a continuous nebula spread throughout the equatorial plane.

In 1973, Prentice pointed out that if the interior of the proto-solar cloud (hereafter PSC) was very strongly convective such that in the cool outer layers the convective motions had mean radial speeds $\langle v_t \rangle$ that were many times larger than the local sound speed $v_s = \sqrt{\gamma \mathcal{R} T/\mu}$, then these motions create a turbulent radial stress in the gas, denoted by $\langle \rho_t v_t^2 \rangle$, which cannot be ignored. This stress can be much larger than the local gas pressure $p_{\text{gas}} = \rho v_s^2/\gamma = \rho \mathcal{R} T/\mu$. Here ρ, T, μ are the local average gas density, temperature and molecular weight, ρ_t is the mass density of moving material, γ is the ratio of specific heats and $\mathcal{R}$ is the universal gas constant. As the convective motions are driven by buoyancy, a simple scaling argument leads to the formula

$$\langle \rho_t v_t^2 \rangle = \beta \rho GM(r)/r \tag{2}$$

This expression is valid for a non-rotating cloud. Here $M(r)$ denotes the mass interior to radius r, G is the gravitation constant, and β is a dimensionless constant called the turbulence parameter. The total radial stress at any point in the cloud is then given by

$$p_{\text{tot}} = \rho \mathcal{R} T/\mu + \beta \rho GM(r)/r \tag{3}$$

At the center of the cloud, $M(0) = 0$, T is a maximum and the turbulent stress is zero. At the surface $M(r)$ achieves its maximum value, T is least and the ratio $F_t = \left\langle \rho_t v_t^2 \right\rangle / p_{\text{gas}}$ of turbulent stress to gas pressure is greatest. Thus F_t increases steadily with increasing radius r. In other words, the inclusion of turbulent stress leaves the central region of the cloud unchanged but pushes the tenuous outer layers outwards. This causes the moment-of-inertia factor f to fall. Typically for a cloud of molecular H_2, f drops from ~0.112 to a plateau level of 0.010 as β increases from 0 to 0.1 (Prentice, 1973). When rotation of the cloud is included, f falls by a further factor of $(1+\Theta_e/2)^2$, where $\Theta_e = \omega_e^2 R_e^3 / GM_e$ denotes the ratio of centrifugal force to gravitational force at the equator and ω_e is the angular frequency.

Thus the inclusion of turbulent stress dramatically lowers the cloud's moment-of-inertia factor, so accounting for the low masses of the planetary/regular-satellite systems relative to their primary bodies, as quantified in equation (1) and also equation (4) below. Prentice (1978a, 1978b) has also demonstrated that (i) thermally-driven convective motions create a turbulent viscosity η_t in the gas. This viscosity is essential for the cloud to rotate nearly uniformly and so efficiently convey angular momentum from the centre to its edge. And (ii), that the breakdown of convective transport above the photosurface of the cloud leads to a scaling down of the turbulent stress there and the onset of a steep density inversion where the total pressure remains nearly constant. The highly turbulent

interior of the cloud is thus capped with a dense shell of non-turbulent gas whose density exceeds that of the gas at the photosurface level by a factor $(1+F_t) \sim 30$.

The net result of the density inversion above the photosurface is that the turbulent cloud is able to store far more material at its edge than the non-turbulent structure. As the proto-solar cloud contracts inwards through the orbital radius $R_e = R_0$ of Neptune, where $\Theta_e(R_0)=1$, a dense equatorial belt of non-turbulent gas is left behind, so forming the first orbiting gas ring. Its angular velocity ω_0 at radius R_0 matches the local Keplerian frequency $\omega_{\mathrm{Kep}} = \sqrt{GM_0/R_0^3}$. The subsequent process of pressure restoration in the outer layers of the cloud then causes Θ_e to drop catastrophically to a new solution value $\Theta_1^{'} < 1$. The equator of the cloud re-establishes itself at a new finite radius $R_1^{'} = \frac{2}{3}R_0\left(1+\Theta_1^{'}/2\right)$. The contracting proto-solar cloud thus abandons a discrete family of orbiting gas rings at orbital radii $R_n\ (n=0,1,2,\ldots)$ which satisfy the equations

$$R_n/R_{n+1} \approx \left[1+\frac{m_n}{M_n f_n}\right]^2 \tag{4}$$

Here m_n denotes the ring mass and M_n the residual cloud mass after detachment of the nth gas ring. If the contraction of the cloud mass occurs homologously, so that m_n/M_n and f_n stay reasonably constant, then the R_n form a geometric sequence akin to the Titius-Bode law of planetary distances.

We now apply equation (4) to the system of Galilean satellites, for which the observed mean geometric spacing ratio is $\langle R_n/R_{n+1}\rangle = 1.647$. Setting $M_n = M_J$, where $M_J = (1.89861 \pm 0.00024)\times 10^{27}$ kg is Jupiter's mass (Anderson *et al.*, 1996a) and taking $\langle f_n\rangle = 0.02$, we obtain a mean gas ring mass $\langle m_n\rangle = 1.075\times 10^{25}$ kg. Assume, for the moment, that the gas consists of H_2, He and other elements in solar proportions, as compiled by Anders and Grevesse (1989) and Grevesse *et al.* (1992) and discussed in more detail below in Section 3. In that case, the total mass of condensable rock and H_2O ice in each ring is

$$m_{\text{rock}} \approx 5.3\times 10^{22} \text{ kg}$$
$$m_{H_2O} \approx 8.3\times 10^{22} \text{ kg}$$

Hence if the system of Galilean satellites did condense from rings of gas of roughly equal mass—dictated by the need for the proto-Jovian cloud to shed excess spin angular momentum during its inward radial contraction from the orbit of Callisto—we should expect to see rocky satellites of mass $\sim 5\times 10^{22}$ kg and rock + ice satellites of mass $\sim 13\times 10^{22}$ kg. Quite remarkably, the mass of the mostly rocky Europa is about this amount, namely 4.8×10^{22} kg, and the mean of the masses of the two, rock+ice moons, Ganymede and Callisto, is 12.8×10^{22} kg.

It is extraordinary, therefore, how successful the modern Laplacian theory of solar system origin is able to account quantitatively even at the simplest level for both the broad orbital

structure and distribution of mass in the Jovian system. This very satisfying feature was first noted by Prentice and ter Haar (1979).

3. Gravitational contraction and thermochemical development of the proto-solar cloud

3.1 Rate of radial contraction

Consider now the physical structure and thermochemical evolution of the PSC during its gravitational contraction from an estimated initial radius $R_i = 7500 R_\odot$. This value exceeds Neptune's mean orbital radius $R_0 = 6463.2 R_\odot$ ($R_\odot = 6.9598 \times 10^5$ km). It is assumed that for equatorial radii $R_e < R_i$, the cloud is sufficiently opaque that a convective equilibrium is established throughout its interior. The formation of a small central core of stellar density and mass $\sim 0.044 M_\odot$ is needed to release sufficient energy so that the levels of dissociation of H_2 and ionization of H and He throughout the rest of the cloud match the local thermodynamical equilibrium values (Prentice, 1978b). Here $M_\odot = 1.98892 \times 10^{30}$ kg is the solar mass (Standish, 1990), taking $G = 6.67259 \times 10^{-20}$ $km^3\ s^{-2}\ kg^{-12}$ (Cohen and Taylor, 1987). If the existence of the central core is ignored, then a full Kelvin-Helmholtz equilibrium cannot be achieved until the cloud radius R_e has shrunk to the value $R_* = 202.2 R_\odot$, for the values of the other parameters given below. The rate of radial contraction for radius $R_e \le R_*$ is determined from the equation $\mathcal{L} = 2.8113 \sigma_s R_e^2 T_e^4 = -d\mathcal{E}_{tot}/dt$. Here σ_s is the Stefan-Boltzmann constant and $\mathcal{L}$ denotes the luminosity of the fully rotating PSC whose shape is lenticular, with polar

radius $R_p = \frac{2}{3} R_e$. Also, $\mathcal{E}_{\rm tot}$ denotes the cloud's total energy, including both the gravitational potential energy and dissociation/ionization energies. At radius R_*, $dR_e/dt = -2.166 \times 10^{-5} v_{\rm Kep}$, where $v_{\rm Kep} = \sqrt{GM_*/R_*}$ is the local Keplerian velocity for cloud mass $M_* = 1.0935 M_\odot$. Since $T_e \propto R_e^{-0.9}$ and, fairly closely, $d\mathcal{E}_{\rm tot}/dt \propto \left(GM_e^2/R_e^2\right) dR_e/dt$, it follows that

$$\nu_e(R_e) \approx 0.00377 (R_e/R_\odot)^{0.4} \quad R_\odot/\mathrm{yr}$$

The cloud thus takes 8.3×10^4 yr to contract from size R_i to R_*. The contraction time from the orbit of Neptune to Mercury is 8.0×10^4 yr. In contrast, the contraction from Mercury's orbit to radius $R_e = 1.5\ R_\odot$ is much slower, taking $\sim 10^7$ yr.

3.2 Angular momentum evolution and mass loss

Next, we consider the physical structure and angular momentum evolution of the PSC. These are controlled by four parameters. The first of these is the initial cloud mass M_i prior to the shedding of the first gas ring, supposed at the orbit of Neptune. This is chosen so that the final cloud mass, at orbital radius $R_e = 1.5\ R_\odot$, is $M_\odot$. The second parameter is the polytropic index n_1 of the super-adiabatic convective core of the PSC in which H is wholly atomic. Suppose n_1 is treated as a variable and allowed to fall below the adiabatic value 1.5 and that the polytropic index n_2 of the outer molecular layer is reduced by the same amount also. Then the gas pressure p_n on the mean orbit of the gas ring shed at the orbit of Mercury increases relative to that for a purely adiabatic cloud.

For gas ring temperatures in the vicinity of 1640 K, this increase in pressure increases the separation between the condensation temperatures of Fe–Ni alloy and $MgSiO_3$–Mg_2SiO_4 silicates (Grossman, 1972; Lewis, 1972). As a consequence, the condensate is starved of silicates relative to metals and so has a higher mean density (Prentice, 1991, 1995). Setting $n_1 = 1.1$, the mean density of the condensate matches the observed uncompressed mean density of Mercury, namely ~5.3 g/cm^3 (Anderson *et al.*, 1987).

The next parameter is the turbulence parameter β. A value $\beta \geq 0.05$ensures that the cloud sheds discrete gas rings during its gravitational contraction. The choice $\beta = 0.08475$ causes the peak in the condensate mean density due to the metal/silicate fractionation process to occur exactly at Mercury's orbit. Lastly, there is the ratio $\theta_{\rm ph} = \left[T_{\rm ph} / T_c\right] / \left[\mu_{ph} / \mu_c\right]$ of the photo-surface temperature to central temperature, divided by the corresponding ratio of molecular weights. Setting $\theta_{\rm ph} = 0.0027703$, the mean ratio $\left\langle R_n / R_{n+1} \right\rangle$ of the orbital radii of adjacent gas rings between the orbits of Neptune to Mercury matches the observed mean value, namely 1.7231. For the above choices of n_1, β and $\theta_{\rm ph}$, we obtain $M_i = 1.169\ M_{\odot}$,. The PSC thus loses some ~15% of its mass during its contraction from Neptune's orbit to present solar size.

3.3 Methane and carbon synthesis in the outer layers

During the homologous contraction of the PSC, the temperature at the equator scales closely as $T_e \propto R_e^{-0.9}$. The temperatures T_n of the gas rings shed at the orbits of

Neptune, Uranus, Saturn and Jupiter are shown in Table 1. The corresponding gas p_n on the mean orbit of each ring are also shown. Within the outer layers of the PSC, the temperature and gas pressure increase with depth according to the super-adiabatic law $p \propto T^{2.9426}$. Thus although at the surface of the cloud it is far too cold for any synthesis of methane CH_4 and C(s) solid carbon from the initial store of CO, this is not the case within the warm interior. As a consequence and as explained in detail elsewhere (Prentice, 1993), at sufficient depth inside the cloud CH_4 and, in some instances C(s), can be produced from CO and CO_2 through catalytic synthesis on the surfaces of Fe–Ni grains. Some 49.5% of the Fe is available as catalyst at the assumed nominal synthesis temperature $T_{cat} = 475$ K, after allowance is made for FeS formation. The reaction products are then assumed to be advected to the surface unchanged. It is assumed that the rapid inter-conversion between CO and CO_2 continues down to a quench temperature $T_q = T_{cat} - 50$ K. The production rate of NH_3 from N_2 is negligible at temperature T_{cat} for the low gas pressures of the outer layers of the PSC. (*cf.* Lewis and Prinn, 1980). As a consequence, all N remains as N_2.

Table 1 lists the distribution of carbon number in the four gas rings shed by the PSC at the orbits of Neptune, Uranus, Saturn and Jupiter. The contraction time t_n from the initial cloud radius $R_i = 7500\ R_\odot$ to orbital radius R_n is also given. The main point to note from this table is the steady conversion of CO and CO_2 to CH_4 in the outer layers of the PSC during cloud contraction. By the time the cloud has shrunk to the orbit of Jupiter, 91% of

the carbon has been converted to CH_4. Another point to note is the production of C(s). This is a transient phenomenon and only occurs for large cloud radii, where the outer layer gas pressures are very low. By the time the cloud has shrunk to equatorial radius $R_e \approx 870\ R_\odot$, all C(s) has gone. The condensate which forms at the orbit of the main-belt asteriods, i.e. at radius 605 $R_\odot$, is thus expected to be free of carbon (and also water ice). That is, the original population of planetesimals which condensed at the mean orbit of the asteroids was entirely stony. Inward orbital diffusion of carbon-bearing planetesimals at Jupiter's orbit is needed account for the carbonaceous character of the outer asteroid population.

4. Formation of the Proto-Jovian Cloud

4.1 Condensation of the proto-solar gas ring at Jupiter's orbit

Consider now the gas ring of mass 1.56×10^{28} kg that is shed by the PSC at Jupiter's orbit. It consists chiefly of H_2 and He. All other elements are present in solar proportion (Anders and Grevesse, 1989; Grevesse *et al.*, 1992). Knowing the elemental abundances, we can construct the standard solar chemical mix, in which the elements are sorted into broad composition categories. This is given in Table 2. The total rock mass fraction is $X_{\text{rock},\odot} = 0.004968$.

It is now assumed that chemical condensation into solid grain occurs in accordance with the equilibrium condensation models first proposed by Larimer (1967), Lewis (1972) and

Grossman (1972). A computational code has been specifically developed to deal with the gas ring configuration of the modern Laplacian theory of solar system origin (Prentice, 1978a, 1990, 1991, 1995). At Jupiter's orbit, the temperature of the gas ring at the moment of detachment from the PSC is 158.5 and the gas pressure on the mean orbit is 1.64×10^{-6} bar. For these parameters, the condensate consists simply of rock (mass fraction 0.6519), graphite (0.0146) and water ice (0.3335). The rock consists of $MgSiO_3$ (rock mass fraction 0.2568), Mg_2SiO_4 (0.1800), SiO_2 (0.0579), $Ca_2MgSi_2O_7$ (0.0423), $MgAl_2O_4$ (0.0309), FeS (0.2044), Fe_3O_4 (0.1755), and NiS (0.0229). The balance of the rock, making up mass fraction 0.0293, consists of NaOH, KOH, Cr_2O_3, P_2O_5, TiO_2, V_2O_5, MnS, ZnS, NaCl, CaF_2, Co, Cu and residuals).

Comparing the rock and ice mass fractions above with those of the standard solar mix, it is clear that the condensate at Jupiter's orbit is water deficient by a factor of about 3 relative to solar abundance. The reason for this shortfall is that the temperature of this proto-solar gas ring is just 5.1 K less than the condensation temperature of H_2O on the mean orbit. Thus only 33.5% of the available water vapour of the gas ring can condense as ice. Allowing for the formation of NaOH and KOH, the net condensed mass of H_2O is a fraction $\phi_{H_2O}=0.3495$ of the initial free H_2O vapour mass. Hence the very same process of chemical fractionation which operated in the gas ring at Mercury's orbit,

causing a shortfall in the condensed mass fraction of silicates relative to metal there, also operates with the same effect on the ice and rock mass fractions at the orbit of Jupiter.

4.2 Formation of a planetary core

After chemical condensation into solid grains has occurred, the grains migrate from all regions of the residual gas ring onto its mean orbit to form a concentrated torus. This process is depicted in Figure 2. Self-gravitation within the grain torus results in the formation of planetisimals which remain bound to the mean orbit through the combined action of gas drag and the gravity of the PSC. These processes have been examined elsewhere (Prentice 1978a, 1980; Hourigan, 1997). The process of accumulation of the first generation of planetisimals to a single orbiting planetary core remains a largely unexplored aspect of the modern Laplacian theory.

The total mass of condensate at Jupiter's orbit is 19.9 $M_{\oplus}$. Assume now, in line with the calculations of Mizuno (1980) and others, that the first stage of Jupiter's formation was the accumulation of a solid planetary core of mass roughly 15 $M_{\oplus}$. This core then serves as sink for capturing the light gases and residual solids of the gas ring at Jupiter's orbit. These solids are easily captured since they form a concentrated slurry along the mean orbit. In contrast, probably only a small fraction of the gas can be captured because of radial dispersal due to viscous forces induced by the steep gradient of the orbital angular velocity distribution in the initial gas ring. We have $\omega(s,z)=\omega_0(R_0/s)^2$. Here (s,z)

refer to cylindrical polar coordinates, $s = R_0$, and $z = 0$ defines the mean orbit, as shown in Figure 2, and ω_0 is the angular velocity on the mean orbit.

4.3 Composition of the primitive Jovian atmosphere

Hence the primitive Jupiter probably consisted of a heavy-element core of mass $m_{core} \approx 15 M_\oplus$ surrounded by a radially extended envelope of mass $m_{\rm env} \approx 320 M_\oplus$, containing ~$5M_\oplus$ of the condensate mix defined above, along with the uncondensed chemical constituents of the proto-solar gas ring, namely H_2, He, Ne, Ar, N_2 and CH_4, and including the remaining H_2O vapour of mass ~$1.6M_\oplus$. This data imply a rock mass fraction $Z_{\rm rock} \approx 0.010$ and total H_2O mass fraction $Z_{H_2O} \approx 0.010$. Comparing these fractions with the solar abundances given in Table 2, we see that the rock is enhanced by a factor of 2 and H_2O by a factor of 1.3, relative to solar expectations.

On the basis of the above model for Jupiter's formation, Prentice (1996a) predicted that the sulphur content of the Jovian atmosphere to be twice solar, yielding a H_2S to H_2 number ratio $n_{H_2S} / n_{H_2} = 7.4 \times 10^{-5}$. This prediction was subsequently confirmed by the Galileo Probe. In their initial report, Niemann *et al.* (1996) found that $\left[n_{H_2S} / n_{H_2} \right]_J = (7.7 \pm 0.5) \times 10^{-5}$. This result is a very significant triumph for the modern Laplacian theory since H_2S is a true indicator of the heavy element abundance of

the Jovian atmosphere. The H_2S measurement has been re-confirmed by subsequent re-analysis of the Probe data (Niemann *et al.*, 1998). Although the Galileo Probe measurements were unable to give any estimate of the global H_2O abundance, the predicted enhancement of 1.3 times solar abundance made by Prentice (1996a) is consistent with the 1–2 times solar value deduced indirectly from meterological considerations (Showman and Ingersoll, 1998). The predicted near solar abundance for He has also been confirmed by the Probe data (Zahn *et al.*, 1998), but the ~3 times solar abundance of CH_4 still remains unexplained.

Lastly, in quantifying the chemical composition of the proto-Jovian envelope it is convenient to let $\zeta_{\rm en} \approx 2$ denote the enhancement in abundance of fully condensed species relative to solar abundances in the material captured from proto-solar orbit. Rock is thus enriched by factor $\zeta_{\rm en}$, while the unnormalized H_2O abundance is given by

$$X_{\rm J}(H_2O) = \left(1 + (\zeta_{\rm en} - 1)\phi_{H_2O}\right) X_{\odot}\,(H_2O) \qquad (5)$$

where $\phi_{H_2O} \approx 0.3495$ is the fraction of condensed H_2O in the proto-solar gas ring. Choosing $\zeta_{\rm en} = 2.0812$, the H_2S to H_2 number ratio in the proto-Jovian envelope exactly matches the Probe measurement. Table 3 gives the predicted broad chemical composition of the proto-Jovian atmosphere for this choice of $\zeta_{\rm en}$. Because of the high gas pressures in this atmosphere compared to those of the PSC, it is safe to assume that all incoming C(s), CO and CO_2 are converted to CH_4, and all N_2 to NH_3 (Lewis and

Prinn, 1980). The abundances of both C and N in the proto-Jovian atmosphere are again expected to be nearly solar. The H_2O abundance of the Jovian atmosphere is now 1.35 times solar for this choice of ζ_{en}.

5. Gravitational contraction of the Proto-Jovian cloud

We are now in a position to model the contraction of the proto-Jovian cloud (hereafter PJC). Since the orbit of the outermost regular satellite Callisto is 26.34 R_J, where $R_J = 71{,}492$ km is the 1-bar equatorial radius of Jupiter (Davies *et al.,* 1992), it is reasonable to assume an initial equatorial radius for the PJC, $R_e = R_i \sim 50R_J$. The cloud is assumed to acquire a super-adiabatic convective equilibrium at that radius through heat generated by gravitational contraction. We also assume that the orbit of Callisto marks the radius R_0 where the centrifugal force at the equator of the PJC first matches the gravitational force and a gas ring is shed. Thereafter, during subsequent contraction, we assume that gas rings are shed close to the present mean orbital radii of the other large satellites at the time of detachment from the cloud. Next, in computing the structure of the PJC, we adopt the same values for the parameters β and n_1 that were derived for the PSC, namely $\beta = 0.08475$ and $n_1 = 1.1$. The parameter $\theta_{ph} = 0.0049066$ is chosen, as before, so that the mean geometric ring spacing ratio $\langle R_n/R_{n+1} \rangle$ matches the observed value, *viz.* 1.6465. The initial cloud mass is $M_i = 1.0542M_J$. The contraction occurs nearly homologously from radius R_i to $3R_J$. A steady but modest departure from uniformity occurs through the progressive dissociation of H_2 in the cloud interior. The

temperature $T_{\rm ph}$ at the photosurface increases closely as $T_{\rm ph} \propto R_e^{-0.9}$, ignoring solar radiation. Allowing for heating due to the primitive sun, whose estimated luminosity is $\mathcal{L}_i \approx 0.7\mathcal{L}_\odot$, the background temperature at Jupiter's orbit for an assumed albedo of 0.5 is $T_{\rm b} \approx 93.8$ K. The effective mean temperature of a gas ring at the moment of detachment from the PJC is then

$$T_n = T_{\rm eff} = \left(0.5T_{\rm ph}^4 + T_{\rm b}^4\right)^{0.25} \tag{6}$$

The factor of 0.5 multiplying $T_{\rm ph}^4$ in equation (6) is a geometric factor associated with the fact that the surface area for radiance from a gas ring of given minor radius is twice the area receiving energy from the PJC.

For cloud radii $R_e = 3R_{\rm J}$, $T_{\rm eff} = 898$ K. Since further homologous contraction results in unreasonably large $T_{\rm eff}$ it is assumed that for $R_e \leq 3R_{\rm J}$, β begins to decline in a manner such that the cloud's moment-of-inertia factor stays constant, namely $f = 0.03875$ while $T_{\rm eff}$ smoothly passes to a final cloud temperature $T_{\rm end} = 750$ K, corresponding to radius $R_e = 1.5R_{\rm J}$. The solid heavy curve in Figure 3 gives the plot of the effective blackbody temperature $T_{\rm eff}$ at the equator of the PJC as a function of the cloud equatorial radius $R_{\rm eq} \equiv R_e$. The open circles mark the temperatures of the gas rings cast off at the orbits of the four Galilean satellites. The lighter curves define the condensation temperatures of the major chemical constituents on the mean orbit of the locally detached gas rings, plotted against cloud radius $R_{\rm eq}$. These curves correspond to the choice $\zeta_{\rm en} = 2$. They are

barely distinguishable from those for the case $\zeta_{en} = 2.0812$ which is adopted for the rest of the paper.

Table 4 gives the gas ring temperatures T_n, mean orbit pressures p_n and detachment times for the four Galilean gas rings, along with the broad chemical composition of the condensate and both the total mass of condensate and its mean specific density ρ_s. This last quantity is calculated for temperature 298.15 K and 1 bar pressure.

6. Chemical condensation of the Galilean satellites

6.1 The general picture

Inspecting Figure 3 and Table 4 we observe that the gas ring model of planet/satellite formation does a very good job of explaining the broad chemical structure of the Galilean satellite system. As one passes from the orbit of Io to Callisto, the mean density of the condensate declines with increasing orbital radius in a manner that closely replicates the observed trend in satellite mean density, which is shown in Table 5. The agreement is even better after allowance is made for the effects of self-compression (see section 8). The condensation point of water ice lies about midway between the orbits of Europa and Ganymede. This explains the sharp drop in mean density between the inner and outer pairs of satellites. The condensation model thus suggests that Europa possessed no initial store of H_2O ice, while Ganymede and Callisto acquired roughly equal proportions of rock and ice. In addition, Callisto contains some 5% by mass of NH_3 incorporated in the condensate as the mono-hydrate ice $NH_3 \cdot H_2O$.

It is remarkable that the same choice of turbulence parameter β which accounts for the broad chemical structure of the planetary system, also accounts for that of the Galilean system. There is, however, one problem with Table 4 in that the predicted mass of condensate in each gas ring is about twice the observed satellite mass. These are listed in Table 5. This means that either the efficiency of the gravitational accumulation process was only 50% or, more likely, that the real structure of the proto-Jovian cloud and its family of gas rings is not completely represented by the simple model for the radial turbulent stress, expressed in equation (2). That is, the gas ring masses may be overestimated by a factor of two. An attempt to improve the theory of supersonic turbulent convection especially to model the degradation of turbulent stress in the outer layers of the cloud is being currently undertaken. This study takes into accout the results of a detailed numerical simulation of supersonic turbulent convection in a model solar atmosphere (Dyt, 1997; Dyt and Prentice, 1998).

6.2 Iron-rich Io

Table 6 gives a breakdown of the predicted rock constituents of each of the Galilean satellites. Io rock differs markedly from that of the other three satellites, which are all very similar in composition. It is much drier, containing only some 0.5% by weight H_2O tied up in tremolite. A second important difference with Io lies in the distribution of iron. All of the satellites have a common supply of FeS which accounts for roughly 50% of the Fe atoms. For the outer three moons, the remaining iron is all present as Fe_3O_4. For Io,

the gas ring is too hot for Fe to be rusted by water vapour to form Fe_3O_4. Instead, fayalite (Fe_2SiO_4) appears forms via the solid-state diffusion reaction.

$$2Fe(s) + SiO_2(s) + 2H_2O(g) = Fe_2SiO_4(s) + 2H_2(g)$$

This has a formation temperature $T_{form} = 510$ K in the Io gas ring. An alternative reaction path, involving the diffusion of Fe with $MgSiO_3$, cannot proceed here since it has a formation temperature of 420 K (*cf.* Fegley, 1988). Hence there is insufficient $SiO_2(s)$ left after the much swifter tremolite reaction ($T_{trem} = 1000$ K) to use up all the remaining Fe. Allowing for $FeTiO_3$ formation as well, some 16.5% of the initial Fe remains as free metal in Io.

6.3 Europa, Ganymede and Callisto

Consider now Europa, Ganymede and Callisto for which it is argued, as follows, that initially all Mg is tied up chiefly as brucite $Mg(OH)_2$, rather than $MgSiO_3$–Mg_2SiO_4. Within a rising convective updraft inside the proto-Jovian cloud, both MgO(s) and $MgSiO_3(s)$ begin to condense as solid grains as soon as the temperature falls below ~1950 K. MgO(s) is likely to be the dominant condensation product, however, because of the fewer molecular collisions required. Next, $SiO_2(s)$ does not begin to condense until the updraft has cooled to 1850 K. But the time taken for an updraft travelling with the local sound speed $v_s = \sqrt{\gamma p/\rho}$ to pass from the 1950 K to 1850 K radius levels, when the PJC has Europa's orbital dimension, is only 1250 s. Thus whilst it is reasonable to assume that all vapour–vapour reactions, such as $Mg(g) + H_2O(g) \rightarrow MgO(s) + H_2(g)$,

pass to completion in that interval, solid–vapour reactions, such as the reaction $MgO(s) + SiO(s) + H_2O(g) \rightarrow MgSiO_3(s) + H_2(g)$ may not have time to proceed far before the SiO vapour condenses to $SiO_2(s)$. This is because the time-scale for solid–vapour reactions exceed that for vapour–vapour reactions by the collision factor $N_{gr}^{\frac{1}{3}} \sim 10^3 - 10^4$, where N_{gr} is the number of atoms per grain (Fegley, 1988). N_{gr} depends on the grain size a_{gr}. Typically $a_{gr} \approx (0.1\text{–}1)\mu m$. Hence a large portion of the Mg advects to the cloud surface as MgO(s). Since the formation temperature for brucite at Europa's orbit is 414 K (see Figure 3), the conditions are favourable in the outermost cloud layers for the copious hydration of MgO grains. This solid–vapour reaction should proceed far more swiftly than the solid-state reaction $MgO(s) + SiO_2(s) \rightarrow MgSiO_3(s)$ which requires intimate grain contact for long times whilst solid state diffusion takes place.

Returning briefly to Table 6, the last row gives the mean density of the rock condensate calculated at 298.15 K and 1 bar pressure. Amongst the residual rock constituents in each satellite, in order of decreasing abundance, are $MnSiO_3$, Cr_2O_3, P_2O_5 and NaCl. This last mineral makes up 0.16% by mass of Io rock and 0.14% of the other satellites' rock.

7. Construction of thermal and structural models for the satellites

The final stage of this investigation is the construction of detailed thermal evolutionary and structural physical models for each of the Galilean satellites. To this end, two large

computational codes have been developed over the past several years in readiness for the Galileo mission.

7.1 The thermal evolutionary code

The first of the computational codes determines the temporal evolution of the temperature distribution within both homogeneous and differentiated satellites of arbitrary chemical composition. The only heat source considered is radiogenic energy released through the decay of K^{40}, Th^{232}, U^{235} and U^{238}. Io is thus excluded from this study since its heating is derived mostly from tidal action with Jupiter. For simplicity, all satellites are assumed to be solid and, initially, to have a uniform temperature T_s throughout, equal to the present day surface value $T_s = 103$ K (Lupo and Lewis, 1979). The mass and radius of each model are chosen to match the present day values (see Table 5). Empirical formula have been constructed to represent the temperature dependence of the specific heats $C_{p,i}(T)$ and thermal conductivities $\kappa_i(T)$ of the major rock-bearing minerals listed in Table 6, and those of the ices H_2O and NH_3. Here i is the species index. With respect to the minerals, the data compilations of Touloukian *et al.* (1970 a,b) and Robie *et al.* (1978) are very useful. As a rule of thumb, thermal conductivity data is scarce, especially at low temperatures ($T \leq 298.15$ K). It appears non-existent for FeS, NiS, $Ca_2MgSi_2O_7$, $Mg(OH)_2$, NaOH, KOH, and the alkali feldspars $NaAlSi_3O_8$ and $KAlSi_3O_8$ and. To get around this difficulty, a nominal conductivity is prescribed, given by

$$\kappa_i(T) = 4.2\left[\rho_i(298.15)/\rho_{\text{std}}\right]\kappa_2(T)/\kappa_2(298.15) \ \text{Wm}^{-1}\text{K}^{-1} \qquad (7)$$

This formula is based on the standard rock conductivities $\kappa_{std} = 4.2\ \mathrm{Wm^{-1}K^{-1}}$ and specific density $\rho_{std} = 3.5\ \mathrm{g/cm^3}$ adopted by Ellsworth and Schubert (1983). In addition, a temperature dependence on κ_i is the imposed which is the same as that of $MgAl_2O_4$ (i.e., i = 2) (Slack, 1962; Kingery *et al.*, 1954).

Because H_2O ice is a major constituent of Europa, Ganymede and Callisto, it is essential to have accurate thermophysical data for this substance. Table 7 gives empirical representations for $C_p\,(T)$, $\kappa(T)$ as well as those and of other properties of H_2O ice to be used later on. The data used for representing $\kappa(T)$ is in excellent agreement with the more recent low-temperature measurements of Ahmad and Phillips (1987). All of the data in Table 7 is for phase Ih of H_2O ice. Data for the other ice phases does not seem to exist.

It is assumed that all heat is conducted outwards according to the heat diffusion equation

$$\overline{\rho}\overline{C}_p \frac{\partial T_d}{\partial t} = \frac{1}{r^2}\frac{\partial}{\partial r}\left(r^2 \overline{\kappa}\frac{\partial T_d}{\partial r}\right) + H_{\mathrm{nucl}}(t) \qquad (8)$$

Here $T_d(r,t)$ denotes the diffusive temperature at radius r and time t and $\overline{\rho}, \overline{C}_p(T_d)$ and $\overline{\kappa}(T_d)$ are the mean density, specific heat and thermal conductivity. For simplicity, the temperature dependence of $\overline{\rho}$ is ignored at this stage. It is calculated at the adopted reference temperature $T_{\mathrm{ref}} = 200$ K. Within the satellite, only the variation of $\overline{\rho}$ with

changes in composition is taken into account. The volumetric radiogenic heat production rate $H_{\mathrm{nucl}}(t)$ is taken from Turcotte and Schubert (1982, p.140).

Next, $T_d(r,t)$ is compared at each time step with the local solid-state convective creep temperature T_{creep} given by

$$T_{\mathrm{creep}} = \begin{cases} 0.6T_{\mathrm{melt}}(p) & [\text{rock + ice mix}] \\ 1073.15\mathrm{K} & [\text{rock only}] \end{cases} \tag{9}$$

Here $T_{\mathrm{melt}}(p)$ denotes the melting temperature of the major ice component, namely H_2O. It depends on the local pressure $p = p(r)$ which is estimated from a simple integration of the hydrostatic support equation. If $T_d(r,t)$ rises above T_{creep} at any time, we set $T = T_{\mathrm{creep}}$. The 0.6 factor in the creep criterion for ice is taken from Ellsworth and Schubert (1983). The rock creep temperature is from Schubert *et al.* (1979; *cf.* Ransford *et al.*, 1981). Lastly, all satellites are evolved for 4600 Myr. The resulting temperature profile is used in the computation of the internal physical structure.

7.2 The structural code

The computational code for the satellite structure is devised as follows. First the model is divided into distinct compositional zones. Second, the pressure at the boundary between convective and wholly conductive ice zones in the thermal model is used to flag the corresponding boundary in the structural model. The ice zones are then further sub-divided according to the pressure boundaries between the four relevant phases of water ice. These boundaries depend on the local temperature T and are given by the equations

$$
\begin{aligned}
p_{\mathrm{Ih/II}}(T) &= 84.7+8.628T \quad \text{bar} \\
p_{\mathrm{II/VI}}(T) &= 11325.-24.0T \quad \text{bar} \\
p_{\mathrm{VI/VIII}}(T) &= 9636.+41.7T \quad \text{bar}
\end{aligned} \tag{10}
$$

These formulae have been derived by least square fits to the data of Bridgman (1912), Whalley (1969) and Brown and Whalley (1966), respectively. Knowing the temperature profile of T versus p within the thermal model of each satellite, equations (10) then yield a unique solution for each of $p_{\mathrm{Ih/II}}$, $p_{\mathrm{II/VI}}$ and $p_{\mathrm{VI/VIII}}$.

Once all the compositional and phase boundaries are specified, a uniform mean temperature $\overline{T}_j$ is assigned to each zone j. In the case of conductive layers, $\overline{T}_j$ is estimated from the thermal code temperature profile. For convecting layers, $\overline{T}_j$ can be determined by an iterative process within the structure code, by making use of equations (9).

7.3 Computation of specific densities

Lastly, the local density $\rho=\rho(p,T)$ at each point in the satellite model is given by the equation

$$1/\rho(p,T) = \sum_{i=1}^{n} X_i/\rho_i(p,T)$$

where X_i and $\rho_i(p,T)$ denote the mass fractions and specific density of species i and n denotes the total number of species. For rock species, the $\rho_i(p,T)$ are estimated by the semi-empirical formulae

$$\rho_i(p,T) = \rho_i(1,T)\cdot\left(1 + K_0'(p-1)/K_0\right)^{1/K_0'} \qquad (11)$$

Here $\rho_i(1,T)$ denotes the specific density of species i at temperature T and 1 bar pressure, and K_0 and K_0' are the bulk modulus and its pressure derivative at zero pressure and temperature 298.15 K. Space does not permit a full description of these quantities in this paper. However, several important points deserve mention here. First, with regard to $\rho_i(1,T)$ excellent data is given for most rock minerals in Robie *et al.* (1978) for room temperature $T_0 \equiv 298.15$ K. Second, Touloukian *et al.* (1970c) provide an excellent source of thermal expansion data to assist in the computation of $\rho_i(1,T)$ for $T \geq 298.15$. With the exceptions of Fe, Ni, Fe_3O_4 and SiO_2, however, very little thermal expansion data exists for $T < 298.15$. For low temperatures, therefore, a simple extrapolation is assumed via the linear expansion formula

$$(\Delta L)_i / L_0 = B_i\cdot\left(T^{1.7} - T_0^{1.7}\right) \qquad (12)$$

Here $(\Delta L)_i$ denotes the change from the room temperature length L_0 at temperature T. The exponent 1.7 provides a best fit for the Fe thermal expansion data. The coefficient B_i is chosen so that $(\Delta L)_i/L_0$ smoothly matches smoothly onto the high temperature data.

Lastly, a useful compilation of K_0 and K_0' values for several minerals is given in Prentice (1996b). Data for $Mg(OH)_2$ is given in Fei and Mao (1993). Kusaba *et al.* (1997) report improved compressibility data for FeS, especially in regard to two phase transitions of this substance at pressures of 34 kbar and 67 kbar, respectively.

Lupo and Lewis (1979) were the first to provide detailed equations of state [EOS] for the different phases of H_2O ice for use in satellite modelling. Much of the data they assembled, however, pre-dated the advent of X-ray diffraction measurements. Table 8 is an attempt to provide an improved EOS for water ice using the diffraction data. Because of the scarcity of thermal expansion data for the higher pressure phases of ice, it has been necessary to assume that the specific density, $\rho_{H_2O,j}(p,T)$ is a separable function of pressure p and temperature T. Here j is the phase index. A temperature dependence is then imposed which is the same as that of ice Ih, as detailed in Table 7.

8. The satellite models

8.1 Io

The observed mean density of Io, namely 3.529 ± 0.001 g/cm^3 (Anderson *et al.*, (1996b) lies well below the uncompressed *solid* rock density expected at Io's orbit according to Table 6. It would therefore appear that the bulk composition of Io cannot be accounted for by the condensation model presented in this paper. This result is not a surprise however since, as mentioned in Section 1, most scientists agree that at least part of the interior of this volcanically active moon is *molten*. Melting produces a slump in specific density of most rocks, particularly in FeS. Prentice (1996b) thus constructed a pre-Galileo model for Io that is consistent with the observed mean density. All FeS, including dissolved Ni, Cu and Co are accumulated at the centre to form a molten core of

mean density ~4.0 g/cm^3 and mass ~25% of the Io mass. This model yields a predicted mean axial moment-of-inertia coefficient for Io of $f_{\mathrm{Io}} = 0.390 \pm 0.002$.

Now the Galileo Orbiter observed f_{Io} to be $0.378 \pm \begin{matrix} 0.008 \\ 0.007 \end{matrix}$ (Anderson *et al.*, 1996b). This is ~1½σ shy of the predicted value. The real Io thus contains heavier material at its centre—and correspondingly lighter material in its mantle—than that predicted in Prentice (1996b). It is hoped that the revised compositional suite for the initial Io presented in Table 6 may provide the basis of a 4–zone model for Io that is consistent with all of the Galileo gravity data. This model—yet to be constructed—consists of an innermost core of solid Fe-Ni-Co-V (of mass percent ~6% of the Io mass M_{Io}) surrounded by a layer of molten FeS-Cu (mass ~24%), then a layer of molten Fe_2SiO_4 (mass ~12½%) and lastly an outer, iron-free, mantle of calcium and magnesium silicates.

8.2 Europa

Figure 4 shows the internal temperature distribution $T(r,t)$ in Europa (E) plotted as a function of radius r, expressed in units of the satellite radius R_{E} at several chosen times t in the evolution. Starting from an initial uniformly cold state, the interior of the satellite rapidly warms under the influence of radioactive decay. After 500 Myr, the temperature in the core has already reached the value ~800 K where decomposition of brucite $Mg(OH)_2$ can take place (Ransford *et al.*, 1981). We therefore assume that complete dehydration of the initial Europa rock takes place early in the evolution of the satellite,

leading to a present day model consisting of a dehydrated rock core surrounded by an outer mantle of H_2O, including dissolved salt.

If NaOH and KOH are converted to alkali feldspars and all NaCl is evicted with H_2O, then the final mass of the dehydrated rock core is $0.9116M_E$. The rock has the same relative composition as that listed in Table 6 except that the entries for $MgSiO_3$, Mg_2SiO_4, $MgAl_2O_4$ and SiO_2 change to 0.2334, 0.1766, 0.0097 and 0.0000, respectively. $NaAlSi_3O_8$ and $KAlSi_3O_8$ make up a fraction 0.0692 of the total satellite mass. The uncompressed mean density of the new rock at room temperature (298.15 K) and 1 bar pressure—hereafter RTP—is 3.6787 g/cm^3. NaCl makes up 1.63% by mass of the outer H_2O ice mantle of total mass 0.0884 M_E.

The temperatures in the outer layers of the satellite generally peak around time ~1500 Myr. The radius and pressure at the rock/ice boundary are $r_1 = 1415$ km and $p_1 = 2110$ bar. The temperature $T(r,t)$ at that point very quickly rises to the value ~ 151 K where the ice becomes convective. Interestingly, this pressure is very close to the value ~2100 bar where the melting temperature $T_{\rm melt}(p)$ of H_2O ice is a minimum. Thus as physical considerations dictate that $\partial T(r,t)/\partial r < 0$, it is necessary to replace the creep criterion in equation (9) by $T_{\rm creep} = 0.6T_{\rm melt}(p_1)$ in regions where $\partial T_{\rm melt}(p)/\partial p < 0$. At time $t = 4600$ Myr, the thickness of the inner layer of convecting ice is ~ 76 km. This is just half of the total ice layer thickness.

The structural parameters of the computed present-day Europa model are given in Table 9. Figure 5 is a simple schematic picture of the proposed satellite model. The mean density of the 2–zone rock/ice model presented here agrees well with the observed mean density $\overline{\rho}_E = 2.990 \pm 0.046$ g/cm^3, for the satellite radius $R_E = 1565$ km derived from Voyager measurements (Davies *et al.*, 1992). The moment-of-inertia coefficient is also in good agreement with the recommended value of 0.346 ± 0.005 obtained by the Galileo Orbiter gravity experiment (Anderson *et al.*, 1998a). In fact, a value of 0.347 ± 0.004 predicted prior to any of the Galileo flypasts (Prentice 1996c) coincides exactly with the measurement of 0.347 ± 0.014 obtained during the E6 flypast (Anderson *et al.*, 1997a)! Thus a simple 2–zone Europa model, consisting of a dehydrated rock core of mass $0.912M_E$ surrounded by a frozen, salty, H_2O ice mantle of thickness 150 km seems to do a very good job at explaining the Galileo gravity data.

8.3 Ganymede

Consider now Ganymede. Gravity observations by the Galileo spacecraft have confirmed the long-held suspicion that this satellite is a heavily differentiated structure, consisting of a dense rock/metal core surrounded by a thick mantle of H_2O (Anderson *et al.*, 1996a). The gravity data can be accounted by a 2–zone model provided that the uncompressed rock has a density of order 3.6 –3.7 g/cm^3. But the unanticipated discovery of an intrinsic Ganymedan magnetic field by the Galileo magnetometer experiment (Kivelson *et al.*, 1996) favours a 3–zone model in which Fe and FeS have separated out from the

rock to form an inner metallic core. If such a core were molten, then dynamo action within it may generate the observed magnetic field (Schubert *et al.*, 1996).

Prentice (1996c) noted that 2–zone models of Ganymede also have the capacity to produce a native magnetic field if one takes into account a process of thermoremanence within the magnetite constituent of the rock. That is, the release radiogenic heat during the course of Ganymede's evolution causes the temperature in certain parts of the rock core both to rise above and then descend again through the Fe_3O_4 Curie point [$T_C = 858$K]. If this event happened early in the satellite's evolution, at a time when the ancient Jovian magnetic field was, say, 10 times larger than it is today, and as long as this field also remained stable in direction over long periods of time $\sim 10^9$ yr, then thermoremanent magnetization (TRM) of the cooling magnetite may have occurred. The reader is referred to Dunlop and Özdemir (1997, p.5), for an excellent description of TRM. Quite independently, Crary and Bagenal (1996) have also proposed that remanent magnetization may be responsible for Ganymede's magnetic field. In a more recent paper (Crary and Bagenal, 1998), these authors favour a paleomagnetic field arising from dynamo action within previously molten core rather than a background Jovian field as the source of magnetization in Ganymede.

In the present paper it is assumed that Ganymede's observed magnetic field arose from TRM fed by an early, powerful, magnetic field of Jupiter. The calculations are therefore confined to 2–zone models. Further, it will be assumed that the initial Ganymede (G) had

already undergone complete differentiation between its rock and ice phases at the time of its formation, through the disposition of substantial amounts of gravitational accretion energy (Lunine and Stevenson, 1982). Next, as for Europa, it is assumed that the release of radiogenic heat causes a complete dehydration of the rock core, including the eviction of NaCl. From Table 4 and 6, it follows that the mass of the rock core is $0.4786M_G$, while the mass of the ice mantle includes $0.04555M_G$ water of hydration and $0.00075M_G$ of NaCl, in addition to the native ice mass of $0.4751M_G$. That is, the Ganymedean ice is only 9% as salty as that of the Europa's ice mantle. Returning to Table 4, the new mass fractions of $MgSiO_3$, Mg_2SiO_4, $MgAl_2O_4$, SiO_2, and Na-K feldspars, relative to the initial rock mass, are 0.2325, 0.1759, 0.0097, 0.0000 and 0.0689, respectively. The RTP density of the dehydrated salt-free rock core is 3.6758 g/cm^3.

Figure 5 gives the temperature distribution $T(r,t)$ within Ganymede versus internal radius r at various times t in the course of its evolution to present age 4600 Myr. After ~150 Myr, the temperature at the rock/ice boundary at radius $r_1 = 1640$ km rises to the value ~209 K where the ice becomes convective at the pressure $p_1 = 20.2$ kbar at that point. The thickness of the convective layer of ice then grows progressively to ~530 km by 4600 Myr. Unlike the case for Europa, the normal creep criterion given by equation (9) does apply to Ganymede since $\partial T_{\text{melt}}(p)/\partial p > 0$ in the relevant pressure regime. The pressure and temperature at the outer edge of the convective layer are 7.95 kbar and 172 K.

Most of the main parameters of the computed 2–zone structural model for Ganymede are listed in Table 9. The outer mantle of H_2O consists of an inner convective region of mass $0.2453M_G$ and mean temperature 190 K and an outer conductive zone of mass $0.2760M_G$ and mean temperature 130.5 K. The H_2O ice VIII/VI phase boundary lies within the convecting region at the 1715 km radius point. The VI/II and II/Ih phase boundaries are at radii 2200 km and 2556 km.

Comparing the mean density $\bar{\rho}$ of the 2–zone satellite model with the observed value $\bar{\rho}_G = 1.936 \pm 0.022$ g/cm^3 (see Table 5) we see that $\bar{\rho}$ falls short of $\bar{\rho}_G$ by 0.048 g/cm^3, or 2.2 σ. Next consider the mean axial moment-of-inertia factor f. Anderson *et al.* (1996a) report a value $f_G = 0.3105 \pm 0.0028$. Hence the 2–zone model value of 0.3156 exceeds f_G by ~1.8σ. Thus although the parameters of the 2–zone model are not in serious disagreement with the Galileo data, neither are they satisfactory. Suppose now we relax the 2–zone model assumption and introduce a dense inner core of solid FeS at the centre of the satellite. This can be achieved by melting the FeS constituent of the rock (T_{melt} = 1468 K) early in the satellite's radiogenic evolution. A preliminary structure calculation, based on the same thermal profile as the 2–zone model, indicates that if all of the FeS is brought to the centre, then the axial moment-of-inertia factor falls to 0.3106. This is almost the same as f_G. The density of this 2-zone model increases slightly to 1.896 g/cm^3 but it still falls short of the observed value by ~0.040 g/cm^3.

To achieve a model for Ganymede that is consistent with both the observed mean density and axial moment-of-inertia, it is necessary to increase the rock mass fraction of the satellite. According to the condensation model for the Galilean satellites presented in Section 4, the rock mass fraction of Ganymede is controlled by the enhancement factor ζ_{en}. This is the abundance of heavy elements in the primitive Jovian atmosphere, relative to solar abundances. In this paper, the value $\zeta_{en} = 2.08$ was chosen to match the H_2S to H_2 mixing ratio of 7.7×10^{-5} observed in the Jovian atmosphere by the Galileo Probe (Niemann *et al.*, 1996, 1998). If the H_2S to H_2 ratio in the deep atmosphere is $\sim 9 \times 10^{-5}$, as suggested by the data in Figure 6 of Niemann *et al.* (1998) so that $\zeta_{en} \sim 2.5$, the mean density of Ganymede can be accounted by the condensation model presented here. The resulting 3–zone model for Ganymede would consist of an inner dense core of *solid* FeS of mass $\sim 0.116 M_G$, surrounded by an FeS-free rock layer of mass $0.382 M_G$ and an outer, frozen, salty ice mantle of mass $\sim 0.502 M_G$. This model will not be pursued any further here. The conclusion of Anderson *et al.* (1996a) that Ganymede is a 3–zone structure containing an inner metallic core is thus a robust one.

Lastly, we return to the origin of the Ganymedean magnetic field. Figure 7 shows a plot of the temperature at the 1410 km and 1475 km radius points as a function of time. During the radiogenic evolution to present age, the temperature of the rock between these points both rises above and descends through the Fe_3O_4 Curie point. As discussed above, the magnetite constituent of this 65 km thick layer may thus become permanently magnetized through thermoremanent magnetization fed by Jupiter's ancient magnetic

field. Most of the field acquisition took place at a time ~2×10^9 yr. Jupiter's magnetic field must have then been at least one order of magnitude larger than the present day ambient field if we are to account for the strength of the Ganymedan dipole (Kivelson *et al.*, 1996). Figure 8 is a simplified schematic picture of Ganymede, showing the magnetized layer and other principal features of the 2–zone model.

8.4 Callisto

It remains to consider Callisto (C). According to Figure 3 and Table 4, the condensate from which the initial Callisto formed consisted of an intimate mixture of hydrated rock, H_2O ice and $NH_3 \cdot H_2O$ monohydrate. In a pre-Galileo analysis, Prentice (1996a) observed that for the choice of heavy element enhancement factor $\zeta_{en} \approx 2$, the masses of rock and ice in Callisto occur in just the right proportions to produce a chemically uniform satellite model whose mean density $\overline{\rho}$ matched the observed value $\overline{\rho}_C = 1.852 \pm 0.012$ g/cm^3 (see Table 5). On the basis of this good agreement, it was predicted that the satellite had remained cold, structurally unmodified and magnetically inert since the time of its formation (Prentice 1996c). Figure 9 provides a schematic view of this pre-Galileo model of Callisto. The basic structural parameters of the model are also listed in Table 9. In specifying an equation of state for $NH_3 \cdot H_2O$ it is assumed, for simplicity, that this substance behaves like a simple molar mixture of H_2O and NH_3 ices. According to Croft *et al.* (1988), the density of NH_3 ice at 1-bar pressure varies with temperature according as $\rho_{NH_3} = 0.8659 e^{-g(T)}$ g/cm^3, where

$g(T) = 4.198 \times 10^{-7} T^{2.2207}$. The compressibility of NH_3 ice was modelled with data from Stewart (1960).

It was reassuring to learn that the initial gravity measurements of Callisto obtained during the C3 flypast on November 4, 1996, indicated that this satellite does appear to have a chemically undifferentiated structure (Anderson *et al.*, 1997b). Furthermore, the Galileo magnetometer observations indicated the absence of any internal magnetic field (Khurana *et al.*, 1997). More accurate gravity data gathered by the Galileo Orbiter during the C10 flypast of September 17, 1997, has however, produced a substantially revised picture for the internal structure of Callisto (Anderson *et al.*, 1998b). Instead of being chemically homogeneous, as the earlier data indicated, it now seems certain that a partial separation between the rock and ice phases has occurred. The value for the mean axial moment-of-inertia factor f_C obtained from the C10 gravity data is 0.358 ± 0.004. This lies well below the value ~0.384 expected for a chemically uniform rock/ice satellite (see Table 7). Yet despite the gravitational evidence for differentiation, the magnetometer observations still indicate the absence of any central, native magnetic field (Khurana *et al.*, 1998). Most likely, therefore, the core of the satellite is still cold and thermally inactive, as predicted earlier Prentice (1996a,c), and ice is mixed with the rock all the way to the centre.

A new post-Galileo Callisto model has been constructed in which it is assumed that gravitational accretion energy, which had previously been ignored, has melted all the ice

in the outer 34.5% of the mass of the primitive Callisto. The rock component of this melted outer layer then migrated into the frozen inner core. The resulting satellite structure consists initially of a rock-rich, icy core of total mass 0.826 M_C, surmounted by a liquid mantle of H_2O and NH_3. The liquid froze fairly quickly to form an icy mantle of thickness ~270 km. The mass fractions of hydrated rock (the same mixture as in Table 6), H_2O ice and NH_3 ice of the core 0.6000, 0.3623 and 0.0377, respectively. The 1-bar density of the core material at the typical temperature of 200 K is 1.593 g/cm^3. The rock volume fraction $V_{rock} = 0.305$ of the core material is less than the critical value ~0.4 at which the rock/ice mixture becomes too viscous to efficiently convect (Friedson and Stevenson, 1983). We can safely assume therefore that: (i) solid state convection will continue to operate throughout the satellite during the course of its radiogenic evolution to age 4600 Myr, and (ii) that this convection renders the core chemically uniform.

The structural properties of the new, partly differentiated, model for Callisto are given in Table 9. Figure 10 provides a simple schematic of this satellite model. We observe with some excitement that the axial moment-of-inertia factor of this first-try model, namely $f = 0.358$, coincides exactly with the value f_C derived from the Galileo C10 flypast (Anderson *et al.*, 1998b). Clearly the choice $X_{rock} = 0.60$ for the core rock mass fraction proved to be the right one. A larger X_{rock} would have resulted in a smaller f. The central density of the satellite, *viz.* 2.33 g/cm^3, agrees well with the mean core density of 2.3 g/cm^3 estimated by Anderson *et al.* (1998b) for their two-layer model. This excellent

agreement provides a valuable independent check on the validity of the computational scheme for calculating satellite structures which has been presented here.

There is, unfortunately, one major deficiency with one aspect of the proposed new Callisto model, namely that the calculated mean density $\bar{\rho}$ is 0.049 g/cm^3 less than the observed value, namely $\bar{\rho}_C = 1.852 \pm 0.012$ g/cm^3. This happens because the ice is now less compressed than that of the previous homogenous model, since not all of it is subject to the weight of overlying rock. Yet quite remarkably, this shortfall in the $\bar{\rho}$ of the new Callisto model is exactly the same amount as the density shortfall in the Ganymede model presented in Section 8.3. Both satellite models could, therefore, be corrected simultaneously by choosing a larger value for the enhancement factor ζ_{sen} of heavy elements in the primitive Jovian atmosphere, as was discussed in that Section. There is probably no point, however, in carrying out such a refinement in the satellite modelling until all the Galileo data is in. In this regard, it is appropriate now to take into account improved determinations of the satellite mean radii (Davies *et al.*, 1998; Thomas *et al.*, 1998). The calculations reported here have been based on the Voyager determinations (Davies *et al.*, 1992).

9. Conclusions and discussion

We have considered a reformulated version of the original nebula hypothesis of Laplace which includes the influence of turbulent stress $\left\langle \rho_t v_t^2 \right\rangle = \beta \rho G M(r)/r$ arising from supersonic convective motions within each of the primitive contracting clouds which

formed Jupiter and the Sun. This 'modern Laplacian theory' of solar system origin has the capacity to account simultaneously for the observed broad physical and chemical structure of both the planetary and Galilean satellite systems for a single choice of the turbulence parameter β, *viz.* $\beta \approx 0.085$. Furthermore, several key pre-Galileo predictions for the properties of the Jupiter system which were made on the basis of this theory have now been confirmed by the Galileo spacecraft data. These predictions include a 2-fold enhancement of the sulphur abundance in the Jovian atmosphere relative to the solar level of that element, a mean axial moment-of-inertia factor for Europa which coincides exactly with the Galileo Orbiter measurement, and the absence of any native magnetic field of Callisto.

We have suggested that each of the Galilean satellites condensed individually from a concentric family of orbiting gas rings. These rings, each of about the same mass $\sim 1.6 \times 10^{25}$ kg, were cast off by the contracting proto-Jovian cloud close to the present satellite orbits. Setting aside the heat due to the primitive sun, the temperatures T_n of the gas rings vary with mean orbital distance R_n according as $T_n = 197(R_G/R_n)^{0.9}$ K, where R_G denotes Ganymede's present distance. This law, along with a similar scaling law for the gas pressures p_n on the mean orbits, yields a suite of bulk chemical compositions of the condensate in each gas ring whose mean densities closely mimic the observed trend of mean densities of the Galilean satellites. Although Europa condensed above the H_2O ice-point, the condensate rock at its orbit contains a large quantity of the highly hydrous mineral brucite. Early decomposition of this mineral through radiogenic heating created

Europa's present ~150 km thick ice mantle. The condensate at Callisto's orbit includes 4.75% by mass of NH_3.

Detailed thermal evolutionary and physical structural models for each of the 'icy' Galilean satellites were constructed on the basis of the suite of bulk chemical compositions which follow from the above condensation model. By constructing both homogenous and chemically differentiated models, it is possible to infer which satellite structure best explains the Galileo spacecraft observations. A 2–zone model for Europa, consisting of a dehydrated rock core of mass 0.912 M_E and a 150 km thick outer mantle of frozen, salty, H_2O ice is consistent with all of the gravity data. For Ganymede, a similar 2–zone model, based on the initial 52.5% : 47.5% mass proportions of hydrated rock and ice which follow from the condensate model for the heavy-element enhancement factor $\zeta_{en} = 2.08$ in the proto-Jovian cloud, was constructed. This yields a structure whose mean density and axial moment-of-inertia factor are in error by ~2 σ from the observed values. A 3–zone model of Ganymede, containing an inner core of *solid* FeS and a greater total mass fraction of rock, is needed to match all of the data. This may be achieved by assuming a higher value for the heavy element enhancement factor ζ_{en}, namely $\zeta_{en} \approx 2.5$.

It is suggested that Ganymede's native dipole magnetic field was created by thermoremanent magnetization some ~2×10^9 yr after this satellite was formed. This activity took place within a cooling shell of magnetite-bearing rock of radius ~1450 km

and thickness ~65 km. Thermoremanence was fed primarily by Jupiter's early, powerful magnetic field (Prentice 1996c). Ancient dynamo action within the inner core of FeS, which was initially in a molten state, may also have assisted in the field acquisition process.

Lastly, the present work suggests that Callisto is a cold, thermally dormant, and magnetically neutral structure with H_2O and NH_3 ices extending all the way to the satellite centre. The Galileo Orbiter measurements indicate, however, that Callisto is more centrally condensed than a chemically homogeneous body. The gravity data can be accounted for by a modified 2–zone model consisting of a rock-enriched icy core of mass 0.826 M_C (60% hydrated rock, 40% ice) surrounded by a pure H_2O-NH_3 ice mantle of thickness ~270 km. Such a mantle may have formed through melting of the outer satellite layers in the late stages of accretion. If the same process also occurred with Ganymede, the larger mass of this satellite coupled with its higher mass fraction of rock would result in more extensive melting and hence a higher fraction or rock precipitating into the core. Such an event would serve to stymie efficient solid-state convection during the satellite's subsequent radiogenic evolution and so lead to a completely differentiated structure. Thus it was a combination of accretional melting (Lunine and Stevenson, 1982) coupled with a subsequent loss of convective efficiency (Friedson and Stevenson, 1983) which, most likely, determined the different pathways followed by Ganymede and Callisto. In short, Ganymede was 'too big for its boots.' Callisto's capacity to stay cool was also assisted by this moon's greater mass fraction of ice.

Lastly, I note that the very recent discovery by the Galileo magnetometer experiment (Khurana *et al.,* 1998) of a variability in the Jovian magnetic field near Callisto may be accounted for by the proposed store of NH_3. The refreezing of Callisto's initial liquid outer mantle of H_2O-NH_3 results in the formation of a eutectic mixture of H_2O and $NH_3 \cdot 2H_2O$ ices (J.S. Kargel, priv. comm). But the melting temperature of $NH_3 \cdot 2H_2O$ ice is very low, namely $T_m(0) = 176\,\mathrm{K}$ at pressure p = 0 kbar (Hogenboom *et al.*, 1997). It is possible, therefore, that radiogenic heat arising from Callisto's rock-ice core may be just sufficient to maintain a narrow shell of liquid $NH_3 \cdot 2H_2O$ at the pressure depth p ~3 kbar. This depth, where T_m achieves a local minimum ~177 K, lies just outside the dense rock-ice core. Dissolved NaCl in this liquid ammonia dihydrate ocean would then create the electrically conducting layer inferred by the Galileo observations. It was Lewis (1971) who first pointed out that NH_3 may lead to a liquid ocean in Callisto. The present work suggests that Callisto alone possesses an internal ocean. Europa and Ganymede are expected to be frozen solid and Europa's magnetic field, if one exists (Kivelson *et al.*, 1997), arises through thermoremanent magnetization (Prentice, 1996c, 1999).

The Galileo Project has revealed that the Galilean satellite system of Jupiter is remarkably diverse in its physical and chemical structure. The observations have provided valuable clues to the conditions under which this system formed. The model of satellite origin presented here has the capacity to quantify these conditions and appears to

go a long way towards explaining much of the data. Hopefully this work makes a small contribution towards understanding how our solar system came into being.

Acknowledgments

This paper is dedicated to the memory of Sir William H. McCrea, F.R.S., whose good deeds and kindly words served as a source of great inspiration for the past 30 years. The author acknowledges Dr. John D. Anderson (NASA/JPL) for his continued support and hospitality during several visits to the Jet Propulsion Laboratory, Pasadena. Thanks also are due to B. Fegley, Jr., P. D. Godfrey, S. D. Hamann, J. S. Kargel, G. W Null, D. ter Haar, and E. M. Standish for many helpful discussions, and to the Australian Research Council International Researcher Exchange Scheme for travel support.

The research described in this paper was partially carried out at the Jet Propulsion Laboratory, California Institute of Technology, under a contract with the National Aeronautics and Space Administration.

References

Ahmad, N. and Phillips, W. A.: 1987, 'Thermal conductivity of ice and ice clathrate', *Solid State Communications* **63**, 167–171.

Anders, E. and Grevesse, N.: 1989, 'Abundances of the elements: meteoritic and solar', *Geochim. Cosmochim. Acta* **53**, 197–214.

Anderson, J. D., Colombo, G., Esposito, P. B., Lau, E. L., and Trager, G.B.: 1987, 'The mass and gravity field of Mercury', *Icarus* **71**, 337–349.

Anderson, J. D., Lau, E. L., Sjogren, W. L., Schubert, G. and Moore, W. B.: 1996a, 'Gravitational constraints on the internal structure of Ganymede', *Nature* **384**, 541–543.

Anderson, J. D., Sjogren, W. L., and Schubert, G.: 1996b, 'Galileo gravity results and the internal structure of Io', *Science* **272**, 709–712.

Anderson, J. D., Lau, E. L., Sjogren, W. L., Schubert, G., and Moore, W. B.: 1997a, 'Europa's differentiated internal structure: inferences from two Galileo encounters', *Science* **276**, 1236–1239.

Anderson, J. D., Lau, E. L., Sjogren, W. L., Schubert, G., and Moore, W. B.: 1997b, 'Gravitational evidence for an undifferentiated Callisto', *Nature* **387**, 264–266.

Anderson, J. D., Schubert, G., Jacobson, R. A., Lau, E. L., Moore, W. B., and Sjogren, W. L.: 1998a, 'Europa's differentiated internal structure: inferences from four Galileo encounters', *Science* **281**, 2019–2022.

Anderson, J. D., Schubert, G. Jacobson, R. A., Lau, E. L., Moore, W. B., and Sjogren, W. L.: 1998b, 'Distribution of rock, metals and ices in Callisto', *Science* **280**, 1573–1576.

Bridgman, P. W.: 1912, 'Water, in the liquid and five solid forms, under pressure', *Proc. Amer. Acad. Arts. Sci.* **47**, 441–558.

Bridgman, P. W.: 1937, 'The phase diagram of water to 45,000 kg/cm^2', *J. Chem. Phys.* **5**, 964–966.

Brown, A. J. and Whalley, E.: 1966, 'Preliminary investigation of the phase boundaries between ice VI and VII and ice VI and VIII', *J. Chem. Phys.* **45**, 4360–4361.

Campbell, J. K. and Synott, S. P.: 1985, 'Gravity field of the Jovian system from Pioneer and Voyager tracking data', *Astron. J.* **90**, 364–372.

Carr, M. J. and 21 colleagues: 1998, 'Evidence for a subsurface ocean on Europa', *Nature* **391**, 363–368.

Cohen, E. R. and Taylor, B. N.: 1987, 'The 1986 Adjustment to the fundamental physical constants', *Rev. Mod. Phys.* **59**, 1121–1148.

Crary, F. J. and Bagenal, F.: 1996, 'Remanent magnetism and Ganymede's internal magnetic field', *Bull. Amer. Astron. Soc.* **28**, 1075.

Crary, F. J. and Bagenal F.: 1998, 'Remanent magnetism and the interior structure of Ganymede', *J. Geophys. Res.* **103**, 25757–25773.

Croft, S. K., Lunine, J. L. and Kargel, J.: 1988, 'Equation of state of ammonia-water liquid: derivation and planetological applications', *Icarus* **73**, 279–293.

Dantl, G.: 1968, 'Die elastichen moduln von eis-einkristallen', *Phys. Condens. Mater.* **7**, 390–397.

Davies, M. E., Abalakin, V. K., Brahic, A., Bursa, M., Chovitz, B. H., Lieske, J. H., Siedelmann, P. K., Sinclair, A. T., and Tjuflin, Y. S.: 1992, 'Report of the IAU/IAG/COSPAR working group on cartographic coordinates and rotational elements of the planets and satellites: 1991', *Celest. Mech. & Dyn. Astron.* **53**, 377–397.

Davies, M. E., Colvin, T. R., Oberst, J., Zeitler, W., Schuster, P., Neukum, G., McEwen, A. S., Phillips, C. B., Thomas, P. C., Veverka, J., Belton, M. J. S., and Schubert, G.: 1998, 'The control networks of the Galilean satellites and implications for global shape', *Icarus* **135**, 372–376.

Dillard, D. S. and Timmerhaus, K. D.: 1966, 'Low temperature thermal conductivity of solidified H_2O and D_2O', *Pure Appl. Cryogen* **4**, 35–44.

Dunlop, D. J. and Özdemir, Ö.: 1997, *Rock Magnetism: Fundamentals and Frontiers,* Cambridge Univ. Press, United Kingdom.

Dyt, C. P.: 1997, *Numerical simulation of supersonic turbulent convection and its relation to the modern Laplacian theory of solar system origin*, Ph.D. thesis, Monash University, Australia.

Dyt, C. P. and Prentice, A. J. R.: 1998, 'A numerical simulation of supersonic thermal convection', *Mon. Not. Roy. Astron. Soc.* **296**, 56–65.

Ellsworth, K. and Schubert, G.: 1983, 'Saturn's icy satellites: thermal and structural models', *Icarus* **54**, 490–510.

Fegley, B., Jr.: 1988, 'Cosmochemical trends of volatile elements in the solar system', in J. A. Nuth, and P. Sylvester (eds.), *Workshop on the Origins of Solar Systems*, LPI Technical Report 88-04, Lunar and Planetary Institute, Houston, Texas, pp. 51–60.

Fei, Y. and Mao, H-K.: 1993, 'Static compression of $Mg(OH)_2$ to 78 Gpa at high temperature and constraints on the equation of state of fluid H_2O', *J. Geophys. Res.* **98**, 11875–11884.

Friedson, A. J. and Stevenson, D. J.: 1983, 'Viscosity of rock-ice mixtures and applications to the evolution of icy satellites', *Icarus* **56**, 1–14.

Giaque, W. F. and Stout J. W.: 1936, 'The entropy of water and the third law of thermodynamics. The heat capacity of ice from 15 to 273 K', *J. Amer. Chem. Soc.* **58**, 1144–1150.

Ginnings, D. C. and Corruccini, R. J.: 1947, 'An improved ice calorimeter-the determination of its calibration factor and the density of ice at 0°C', *J. Res. National Bur. Stand.* **38**, 583–591.

Grevesse, N., Noels, A. and Sauval, A. J.: 1992, 'Photospheric abundances', in *Proceedings of the First SOHO Workshop,* ESA SP-348, pp. 305–308.

Grossman, L.: 1972, 'Condensation in the primitive solar nebula', *Geochim. Cosmochim. Acta.* **36**, 597–619.

Hobbs, P. V.: 1974, *Ice Physics*, Oxford University Press, London.

Hogenboom, D. L., Kargel, J. S., Consolmagno, G. J., Holden, T. C., Lee, L., and Buyyounouski, M.: 1997, 'The ammonia-water system and the chemical differentiation of icy satellites', *Icarus* **128**, 171–180.

Hourigan, K.: 1977, 'Numerical experiments on planetesimal aggregation during the formation of the solar system', *Proc. Astron. Soc. Aust.* **3**, 169–171.

Jeans, J. H.: 1928, *Astronomy and Cosmogony,* Cambridge University Press, United Kingdom, p. 389.

Kamb, B.: 1964, 'Ice II: a proton-ordered form of ice', *Acta Cryst.* **17**, 1437–1449.

Kamb, B.: 1965, 'Structure of ice VI', *Science* **150**, 205–209.

Khurana, K. K., Kivelson, M. G., Russell, C. T., Walker, R. J. and Southwood, D. J.: 1997, 'Absence of an internal magnetic field of Callisto', *Nature* **387**, 262–264.

Khurana, K. K, Kivelson, M. G., Stevenson, D. J., Schubert, G., Russell, C. T., Walker, R. J., and Polanskey, C.: 1998, 'Induced magnetic fields as evidence for subsurface oceans in Europa and Callisto', *Nature* **395**, 777–780.

Kingery, W. D., Franck, J., Coble, R. L. and Vasilos, T.: 1954, 'Thermal conductivity: X, data for several pure oxide materials corrected to zero porosity', *J. Amer. Ceram. Soc.* **37**, 107–110.

Kivelson, M. G., Khurana, K. K., Russell, C. T., Walker, R. J., Warnecke, J., Coroniti, F. V., Polanskey, C., Southwood, D. J., and Schubert, G.: 1996, 'Discovery of Ganymede's magnetic field by the Galileo spacecraft', *Nature* **384**, 537–541.

Kivelson, M. G., Khurana, K. K., Joy, S., Russell, C. T., Southwood, D. J., Walker, R. J., and Polanskey, C.: 1997, 'Europa's magnetic signature: report from Galileo's pass on 19 December 1996', *Science* **276**, 1239–1241.

Klinger, J. and Neumaïer, K.: 1969, 'Conductibilitié thermique de la glace', *C.R. Acad. Sc. Paris* **269**, Series B, 945–948.

Kusaba, K., Syona, Y., Kikegawa, T., and Shimomura, O.: 1997, 'Structure of FeS under high pressure', *J. Phys. Chem. Solids* **58**, 241–246.

LANDHOLT-BORNSTEIN Numerical Data and Functional Relationships in Science and Technology, New Series: 1975, (Ed. in chief: K-H. Hellwege), *Crystal Structure Data of Inorganic Compounds*, Springer-Verlag, Berlin, Group III, **7**, Part b, pp. 5–7.

Laplace, P. S. de: 1796, *Exposition du Système du Monde*, Courcier, Paris, pp. 387–397.

Larimer, J. W.: 1967, 'Chemical fractionation in meteorites—I. Condensation of the elements', *Geochim. Cosmochim. Acta* **31**, 1215–1238.

Leadbetter, A. J.: 1965, 'The thermodynamic and vibrational properties of H_2O ice and D_2O ice', *Proc. Roy. Soc. (Lond.)* A**287**, 403–425.

Lewis, J. S.: 1971, 'Satellites of the outer planets', *Science* **172**, 1127–1128.

Lewis, J. S.: 1972, 'Metal/silicate fractionation in the solar system', *Earth Planet Sci. Letts.* **15**, 286–290.

Lewis, J. S. and Prinn, R. G.: 1980, 'Kinetic inhibition of CO and N_2 reduction in the solar nebula', *Astrophys. J.* **238**, 357–364.

Lunine, J. L. and Stevenson, D. J.: 1982, 'Formation of the Galilean satellites in a gaseous nebula', *Icarus* **52**, 14–39.

Lupo, M. J. and Lewis, J. S.: 1979, 'Mass-radius relationships in icy satellites,' *Icarus* **40**, 157–170.

Malhotra, R.: 1997, 'Galileo raises new questions about Ganymede', *Physics World* **10**, 21–22.

McKinnon, W. B.: 1997, 'Mystery of Callisto: is it undifferentiated?', *Icarus* **130**, 540–543.

Mizuno, H.: 1980, 'Formation of the giant planets', Prog. Theor. Phys. **64**, 544–557.

Mueller, S. and McKinnon, W. B.: 1988, 'Three-layered models of Ganymede and Callisto: compositions, structures, and aspects of evolution', *Icarus* **76**, 437–464.

Niemann, H. B., Atreya, S. K., Carignan, G. R., Donahue, T. M, Haberman, J. A., Harpold, D. N., Hartle, R. E., Hunten, D. M., Kasprzak, W. T., Mahaffy, P. R.,

Owen, T. C., Spencer, N. W., and Way, S. H.: 1996, 'The Galileo Probe mass spectrometer : composition of Jupiter's atmosphere', *Science* **272**, 846–849.

Niemann, H. B., Atreya, S. K., Carignan, G. R., Donahue, T. M., Haberman, J. A., Harpold, D. N., Hartle, R. E., Hunten, D. M., Kasprzak, W. T., Mahaffy, P. R., Owen, T. C., and Way, S. H.: 1998, 'The composition of the Jovian atmosphere as determined by the Galileo Probe mass spectrometer', *J. Geophys. Res.*, **103**, 22,831–22,845.

Peale, S. J., Cassen, P., and Reynolds, R. T.: 1979, 'Melting of Io by tidal dissipation', *Science* **203**, 892–894.

Prentice, A. J. R.: 1973, 'On turbulent stress and the structure of young convective stars', *Astron. Astrophys.* **27**, 237–248.

Prentice, A. J. R.: 1978a, 'Towards a modern Laplacian theory for the formation of the solar system', in S. F. Dermott (ed.), *The Origin of the Solar System,* John Wiley, New York, pp. 111–161.

Prentice, A. J. R.: 1978b, 'Origin of the solar system: gravitational contraction of the turbulent protosun and the shedding of a concentric system of gaseous Laplacian rings', *Moon and Planets* **19**, 341–398.

Prentice, A. J. R.: 1980, 'Accretion of planetesimals within a gaseous ring', *Aust. J. Phys.* **33**, 623–37.

Prentice, A. J. R.: 1990, 'Iron/silicate fractionation and the formation of the inner planets', *Meteoritics* **25**, 399–400.

Prentice, A. J. R.: 1991, 'Chemical fractionation in gas rings and the formation of the solar system', *Proc. Astron. Soc. Aust.* **9**, 321–323.

Prentice, A. J. R.: 1993, 'The origin and composition of Pluto and Charon: chemically uniform models', *Proc. Astron. Soc. Aust.* **10**, 189–195.

Prentice, A. J. R.: 1995, 'Origin and bulk chemical composition of the terrestrial planets', *Eos Trans. AGU* **76**, F332.

Prentice, A. J. R.: 1996a, 'Origin and bulk chemical composition of the Galilean satellites and the primitive atmosphere of Jupiter: a pre-Galileo analysis', *Earth, Moon and Planets* **73**, 237–258.

Prentice, A. J. R.: 1996b, 'Internal structure and bulk chemical composition of Io: a pre-Galileo prediction', *Phys. Letts. A* **213,** 253–258.

Prentice, A. J. R.: 1996c, 'Origin, thermophysical structure and magnetic properties of the icy Galilean satellites', *Eos Trans. AGU* **77,** F172.

Prentice, A. J. R.: 1999, 'Origin and bulk chemical composition of the Galilean satellites of Jupiter and the inner planets', *30th Lunar Planet Sci. Conf.*, LPI Contribution No. 964, Houston, Texas.

Prentice, A. J. R. and ter Haar, D.: 1979, 'Origin of the Jovian ring and the Galilean satellites', *Nature* **280**, 300–302.

Proctor, T. M.: 1966, 'Low-temperature speed of sound in single-crystal ice', *J. Acoust. Soc. Amer.* **39**, 972–979.

Ransford, G. A., Finnerty, A. A., and Collerson, K. D.: 1981, 'Europa's petrological thermal history', *Nature* **289**, 21–24.

Robie, R. A., Hemingway, B. S., and Fisher, J. P.: 1978, *Thermodynamic Properties of Minerals and Related Substances at 298.15 K and 1 Bar (10^5 Pascals) Pressure*

and at Higher Temperatures, U.S. Geol. Surv. Bull. 1452, U.S. Gov. Printing Office, Washington.

Schatzman, E.: 1949, 'On certain paths of stellar evolution. I Preliminary remarks', *Bull. Acad. Roy. Belgique* **35**, 1141–1152.

Schubert, G., Cassen, P., and Young, R. E.: 1979, 'Subsolidus convective cooling histories of terrestrial planets', *Icarus* **38**, 192–211.

Schubert, G., Zhang, K., Kivelson, M. G., and Anderson, J. D.: 1996, 'The magnetic field and internal structure of Ganymede', *Nature* **384**, 544–545.

Showman, A. P. and Ingersoll, A. P.: 1998, 'Interpretation of Galileo probe data and implications for Jupiter's dry downdrafts', *Icarus* **132**, 205–220.

Slack, G. A.: 1962, 'Thermal conductivity of MgO, Al_2O_3, $MgAl_2O_4$, and Fe_3O_4 crystals from 3° to 300° K', *Phys. Rev.* **126**, 427–441.

Standish, E. M.: 1990, 'The observational basis for JPL's DE200, the planetary ephemerides of the Astronomical Almanac', *Astron. Astrophys.* **233**, 252–271.

Stewart, J. W.: 1960, 'Compression and phase transitions of solid NH_3, SiF_4, H_2S and CF_4', *J. Chem. Phys.* **33**, 128–133.

Thomas, P. C., Davies, M. E., Colvin, T. R., Oberst, J., Schuster, P., Neukum, G., Carr, M. H., McEwen, A. S., Schubert, G., Belton, M. J. S., and the Galileo Imaging Team: 1998, 'The shape of Io from Galileo limb measurements', *Icarus* **135**, 175–180.

Touloukian, Y. S. and Buyco, E. H.: 1970a, *Thermophysical Properties of Matter, Volume 5, Specific Heat: Nonmetallic Solids,* IFI/Plenum, New York–Washington.

Touloukian, Y. S., Powell, R. W., Ho, C. Y., and Klemens, P. G.: 1970b, *Thermophysical Properties of Matter, Volume 2, Thermal Conductivity: Nonmetallic Solids.* IFI/Plenum, New York–Washington.

Touloukian, Y. S., Kirby R. K., Taylor, R. E., and Lee, T. Y. R.: 1970c, *Thermophysical Properties of Matter, Volume 13, Thermal Expansion: Nonmetallic Solids,* IFI/Plenum, New York–Washington.

Turcotte, D. L. and Schubert G.: 1982, *Geodynamics: Applications of Continuum Physics to Geological Problems*, John Wiley, New York, p. 140.

von Zahn, U., Hunten, D. M., and Lehmacher, G.: 1998, 'Helium in Jupiter's atmosphere: results from the Galileo probe helium interferometer experiment', *J. Geophys. Res.* **103**, 22,815–22,829.

Whalley, E.: 1969, 'Structure problems in ice', in Riehl, N., Bullemer, B. and Engelhardt, H. (eds.), *Physics of Ice,* Plenum Press, New York, pp. 19–43.

Whipple, F. L.: 1968, *Earth, Moon, and Planets,* 3rd Edition, Harvard University Press, Cambridge, Mass.

Figure Captions

Figure 1. An artist's visualization of the Laplace's nebular hypothesis of solar system origin. A contracting and rotating gas cloud, originally larger in size than Neptune's orbit, sheds a concentric system of orbiting gas rings. The planets later condensed somehow from the rings. Original drawings due to Scriven Bolton, F.R.A.S. (Whipple, 1968, Fig. 172).

Figure 2. A simple schematic view of a gas ring orbiting the protosun. As the gas cools, solid grains condense out and migrate to the mean orbit of the ring under the combined influence of the protosolar gravity and drag induced by motion through the gas. The mass of gas is much less than the mass M of the protosun and it has uniform specific orbital angular momentum. The orbital angular velocity ω thus varies as $\omega \propto 1/s^2$, where s is the cylindrical distance from the common axis of rotation of the system. On the mean orbit $s = R_0$, ω equals the local Keplerian value $\omega_0 = \omega_{\mathrm{Kep}} = \sqrt{GM/R_0^3}$.

Figure 3. Effective blackbody temperature T_{eff} at the equator of the proto-Jovian cloud (PJC) versus cloud radius R_{eq} which is expressed in units of Jupiter's present equatorial radius $R_{\mathrm{J}} = 71{,}492$ km. The temperatures of the gas rings at the present orbits of the Galilean satellites are shown with the open circles. The other lines in the Figure

give the condensation temperatures of the principal rocks and ices. These are computed for the gas pressure on the mean orbit of the locally detached gas ring.

Figure 4. Internal temperature distribution of a 2–zone model of Europa versus fractional radius $x = r/R_E$ for several key times during the course of its radiogenic evolution to present age (4600 Myr). The satellite model consists of a dehydrated rock core of radius $x_1 = 0.905$ and uniform density 3.68 g/cm^3, capped by a solid H_2O mantle. After time 50 Myr, the temperature at the rock/ice boundary rises to the value $0.6\ T_{melt}\ (p_1) = 151$ K where the ice becomes unstable towards solid-state convection. Here T_{melt} is the melting temperature of H_2O ice and $p_1 = 2.01$ kbar is the boundary pressure. Thereafter the temperature at this boundary stays constant. The surface temperature of the model is set at 103 K throughout the evolution.

Figure 5. Cross-sectional view of the proposed 2–zone model for Europa. A frozen mantle of salty H_2O ice of thickness 150 km and mean temperature 140 K surrounds a dehydrated rock core of mean temperature 680 K. NaCl is the principal salt constituent of the ice. The chief constituents of the rock are FeS, Fe_3O_4, $MgSiO_3$ and Mg_2SiO_4.

Figure 6. Internal temperature profiles of a 2–zone model for Ganymede versus fractional radius $x = r/r_G$ plotted at several times during the evolution to age 4600 Myr. The surface temperature of the satellite is assumed to be constant (i.e., 103 K) throughout the evolution. After time ~ 150 Myr, the temperature T_1 at the grid-point radius

$x_1 = 0.635$ of the rock–core/ice–mantle interface rises to the 0.6 of the local H_2O ice melting temperature $T_{melt} = 345$ K. Thereafter, the ice becomes convective and the temperature at the rock core boundary stays fixed.

Figure 7. The temperature at the fractional radius grid points $x = r/R_G = 0.535$ and $r/R_G = 0.56$ within a 2–zone model of Ganymede plotted as a function of time. Between these two radius points, which are located in the dehydrated rock core, the temperature rises above and then descends through the Fe_3O_4 Curie point during the thermal evolution to present age. Ganymede's observed magnetic field may thus have been created by thermoremant magnetization fed by Jupiter's ancient, but powerful, magnetic field (Prentice, 1996c).

Figure 8. An illustrative summary of the 2–zone structural model for Ganymede. A frozen mantle of H_2O ice of mass 52.1% of the Ganymede mass surrounds a dehydrated rock core. Dissolved NaCl makes up 0.14% of the ice mass. Ganymede's native dipolar magnetic field arises from a 65 km thick shell of rock containing magnetized magnetite.

Figure 9. Cross-sectional view of the internal structure of a pre-Galileo Callisto model consisting of a uniform mixture of hydrated rock, H_2O ice and NH_3 ice. The dashed circles mark the boundaries between the various high pressure phases of H_2O ice. The model remains cool and hence magnetically inert throughout its entire radiogenic evolution through efficient solid-state creep of the ice.

Figure 10. Schematic view of the cross-section of a post-Galileo, partly differentiated model for Callisto's internal structure. A mantle of pure H_2O and NH_3 ices of mass 0.174 times the satellite mass surrounds a denser core containing a uniform mixture of hydrated rock and ices. Solid-state convection of the ice keeps the satellite cool to the centre. The first 90 km of the outer ice mantle is also convective. Although the moment-of-inertia factor of this model matches the Galileo observation (Anderson *et al.*, 1998b), the mean density of the model falls short by 0.05 g/cm^3. A further improvement in modelling is required, especially to allow for $NH_3 \cdot H_2O$ formation, as discussed in Section 9.

Table 1: Physical Characteristics and Carbon Distributions of the Outer Proto-solar Gas Rings

Orbit	Radial distance $R_n/R_\odot$	Elapsed time $t_n/10^4$ yr	Gas ring temperature T_n/K	Gas ring pressure p_n/bar
Neptune	6463	0.80	33.7	8.48×10^{-10}
Uranus	4125	2.81	49.9	5.72×10^{-9}
Saturn	2050	5.05	92.4	1.16×10^{-7}
Jupiter	1118	6.36	158.5	1.64×10^{-6}
	Carbon number fractions			
	f_{CH_4}	$f_{C(s)}$	f_{CO_2}	f_{CO}
Neptune	0.1182	0.0435	0.2256	0.6127
Uranus	0.3905	0.1081	0.1825	0.3189
Saturn	0.7184	0.1089	0.0771	0.0956
Jupiter	0.9093	0.0367	0.0255	0.0285

Table 2: Standard Solar Chemical Mix*

Broad Category	Species	Mass fraction
Gases:	H_2	0.7143498
	He	0.2660000
	Ne, Ar	0.0018185
Ices:	H_2O	7.6877×10^{-3}
	NH_3	1.1297×10^{-3}
	CH_4	4.0459×10^{-3}
Rock oxides :	MgO, Al_2O_3, SiO_2, Fe_3O_4, CaO, TiO_2, Na_2O, K_2O, Cr_2O_3, P_2O_5, V_2O_5	3.7984×10^{-3}
Rock sulphides:	FeS, NiS, MnS, ZnS	1.1560×10^{-3}
Rock halides:	NaCl, CaF_2	8.63×10^{-6}
Unreacted metals:	Co, Cu	4.22×10^{-6}
Rest:		1.1×10^{-6}

*Based on: Anders and Grevesse (1989), Grevesse *et al.* (1992) and the 1987 Atomic Weights.

Table 3: Proposed Broad Chemical Composition of the Proto-Jovian Atmosphere: $\zeta_{en} = 2.0812$

Broad category	Species	Mass fraction
Gases	H_2	0.70846
	He	0.26382
	Ne, Ar	0.00180
Ices	H_2O	1.0373×10^{-2}
	NH_3	1.121×10^{-3}
	CH_4	4.172×10^{-3}
Rocks	Same as Table 2	1.0255×10^{-2}

Table 4. Broad Characteristics of the Family of Proto-Jovian Gas Rings

Orbit	Radial distance R_n/R_J	Elapsed time $t_n/10^6$ yr	Gas ring temperature T_n/K	Gas ring pressure p_n/bar
Io	5.900	6.46	463	18.3
Europa	9.387	5.31	301	2.77
Ganymede	14.973	3.76	199	0.405
Callisto	26.335	1.44	129	0.0399

	Condensate mass fraction			Condensate mass (10^{26} g)	Specific density ρ_s/g cm^{-3}
	Rock	H_2O	NH_3		
Io	1.000	0	0	1.76	3.719
Europa	1.000	0	0	1.88	3.134
Ganymede	0.5249	0.4751	0	3.37	1.477
Callisto	0.4956	0.4569	0.0475	3.33	1.418

Table 5. Bulk Physical properties of the Galilean Satellites

Satellite	Mean physical radius[a] (km)	Mass[b,c] (10^{22} kg)	Mean density (g/cm^3)
Io	1821.3 ± 0.2	8.9319 ± 0.0012	3.529 ± 0.001
Europa	1565 ± 8	4.8000 ± 0.0006	2.990 ± 0.046
Ganymede	2634 ± 10	14.8167 ● 0.0020	1.936 ± 0.022
Callisto	2403 ± 5	10.762 ± 0.005	1.852 ± 0.012

[a] Radii from Davies *et al.* (1992)

[b] Masses: Io (Anderson *et al.* 1996b), Europa (Anderson *et al.*, 1997a), Ganymede (Anderson *et al.*, 1996a), Callisto (Campbell and Synnott, 1985)

[c] Gravitational constant: $G = (6.67259 \pm 0.00085) \times 10^{-20}$ km^3 s^{-2} kg^{-1} (Cohen and Taylor, 1987).

Table 6. Predicted Initial Rock Constituents of the Galilean Satellites

Chemical Species	Mass fractions X_i			
	Io	Europa	Ganymede	Callisto
$Ca_2MgSi_2O_7$	0.	0.0389	0.0387	0.0387
$MgAl_2O_4$	0.0317	0.0284	0.0283	0.0283
$MgSiO_3$	0.1997	0.0003	0.	0.
Mg_2SiO_4	0.1848	0.0002	0.	0.
SiO_2	0.	0.2622	0.2615	0.2615
$Ca_2\ Mg_5\ [Si_8O_{22}](OH)_2$	0.1293	0.	0.	0.
$Mg(OH)_2$	0.	0.2739	0.2733	0.2733
NaOH + KOH	0.0121	0.0108	0.0108	0.0108
Fe	0.0434	0.	0.	0.
FeS	0.2366	0.2068	0.1911	0.1911
Fe_2SiO_4	0.1264	0.	0.	0.
Fe_3O_4	0.	0.1448	0.1574	0.1574
Ni	0.0152	0.0100	0.	0.
NiS	0.	0.0056	0.0209	0.0209
Residuals	0.0208	0.0181	0.0180	0.0180
TOTAL	**1.0000**	**1.0000**	**1.0000**	**1.0000**
Mean density (g/cm^3)	3.7192	3.1342	3.1334	3.1334

Table 7. Thermophysical Properties of H_2O Ice (Phase Ih)

Quantity	Symbol [Unit]	Temperature range [K]	Formula	Data source
Cubical expansion coefficient	$a(T)$ [K^{-1}]	(20, 100.15)	$-6.94 \times 10^{-7} T + 1.0818 \times 10^{-8} T^2$	Leadbetter (1965)
		(100.15, 273.15)	$-3.700 \times 10^{-5} + 7.79 \times 10^{-7} T - 2.022 \times 10^{-10} T^2$	[See also Hobbs (1974), p. 350]
Expansion coefficient integral	$f_1(T) = \int_0^T \alpha(T) dt$	(20, 100.15)	$-3.47 \times 10^{-7} T^2 + 3.606 \times 10^{-9} T^3$	
		(100.15, 273.15)	$7.8 \times 10^{-6} - 3.700 \times 10^{-5} T + 3.895 \times 10^{-7} T^2 - 6.74 \times 10^{-11} T^2$	
Adiabatic compressibility	β_{ad}(T) [bar^{-1}]	(60, 110)	$9.1884 \times 10^{-6} / (1 - 2.7157 \times 10^{-4} T - 1.5988 \times 10^{-6} T^2)$	Proctor (1966)
		(110, 133.15)	$3.2196 \times 10^{-6} + 5.015 \times 10^{-8} T$	[see also Hobbs (1974), p.263]
		(133.15, 273.15)	$1.945 \times 10^{-5} / (1 - 1.7305 \times 10^{-3} t_c - 1.804 \times 10^{-6} t_c^2)$	Dantl (1968)
			$[t_c = T - 273.15]$	[see also Hobbs (1974), p.261]
Specific heat	$C_p(T)$ [kJ / kg.K]	(17, 85)	$-0.13779 + 1.32002 \times 10^{-2} T - 3.23053 \times 10^{-5} T^2$	Giaque and Stout (1936)
		(85, 170)	$-0.78302 + 2.92186 \times 10^{-2} T - 1.65222 \times 10^{-4} T^2 + 3.97284 \times 10^{-7} T^3$	
		(170, 273.15)	$0.12996 + 7.2419 \times 10^{-3} T$	
Thermal conductivity	$\kappa(T)$ [W/m.K]	(16, 100)	$1.605 + 305.3 / T + 9220 / T^2$	Klinger and Neumaïer (1969)
		(100, 273.15)	$0.330 + 525 / T$	Dillard and Timmerhaus (1965)

Table 8. Equation of State of H_2O Ice: $\rho_{H_2O,j}(p,T) = \rho_{H_2O,j}(1,0)e^{-f_1(T)}F_j(p)$

Ice Phase	Index j	Density at 1 bar and 0 K $\rho_{H_2O,j}(1,0)$ g/cm^3	Compression factor $F_j(p)$	Data Source
Ih	1	0.93298*	$e^{\beta_{iso}(p-1)}$, $\beta_{iso}=\beta_{ad}(T)+\alpha_1^2(T)T/\rho_1(1,T)C_p(T)$	Table 6
II	2	1.18066	$e^{\beta_2(p-1)}$, $\beta_2 = 1.21736\times10^{-5}$	Kamb (1964) Bridgman (1912) Landolt-Bornstein (1975, p.5)
VI	3	1.31408	$\left[1-7.5282\times10^{-6}(p-1)+4.068\times10^{-11}(p-1)^2\right]^{-1}$	Kamb (1965) Bridgman (1937) Landolt-Bornstein (1975, p.7)
VIII	4	1.49084	$\left[1-4.3194\times10^{-6}(p-1)^2+2.1036\times10^{-11}(p-1)^2\right]^{-1}$	Bridgman (1937) Hobbs (1974, p.79) Landolt-Bornstein (1975, p.7)

*This value chosen so that $\rho_{H_2O,I}(1, 273.15)$ = g/cm^3 [Ginnings and Corruccini (1947); see also Hobbs (1974, p.346)]

Table 9. Structural Properties of the Computed Satellite Models

Property \ Model	Europa [2-zone]	Ganymede [2-zone]	Ganymede [3-zone]	Callisto [1-zone]	Callisto [2-zone]
Physical radius (km)	1565	2634	2634	2403	2403
Central pressure (kbar)	40.7	74.4	94.0	31.6	34.5
Central temperature (K)	1073	1073	1073	253	263
Central density (g/cm^3)	3.776	3.888	5.607	2.142	2.326
Rock core mean temperature (K)	680	820	820	-	200
Core edge temperature (K)	151	209	209	-	154
Core radius (km)	1415	1640	890/1635	-	2137
Convective boundary (km)	1492	2172	2174	2285	2230
Mean density (g/cm^3)	2.989	1.888	1.896	1.860	1.803
Moment-of-inertia factor	0.3503	0.3156	0.3106	0.3836	0.3580

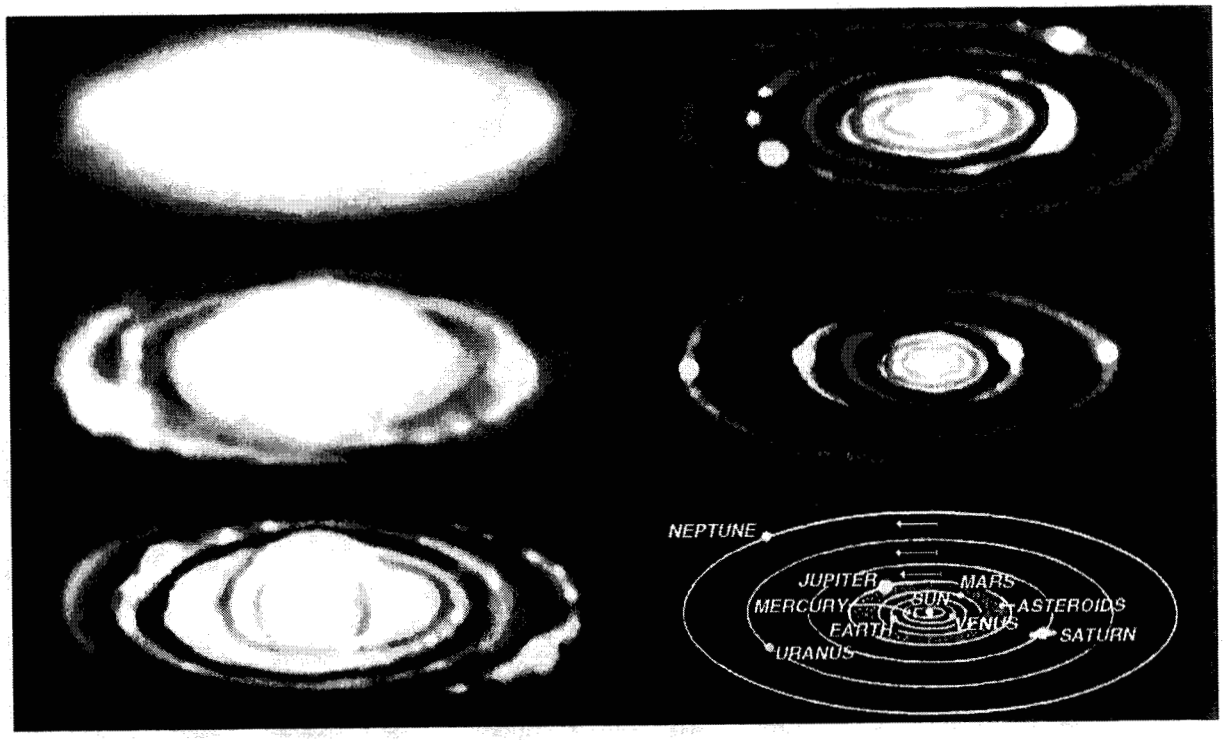

Figure 1

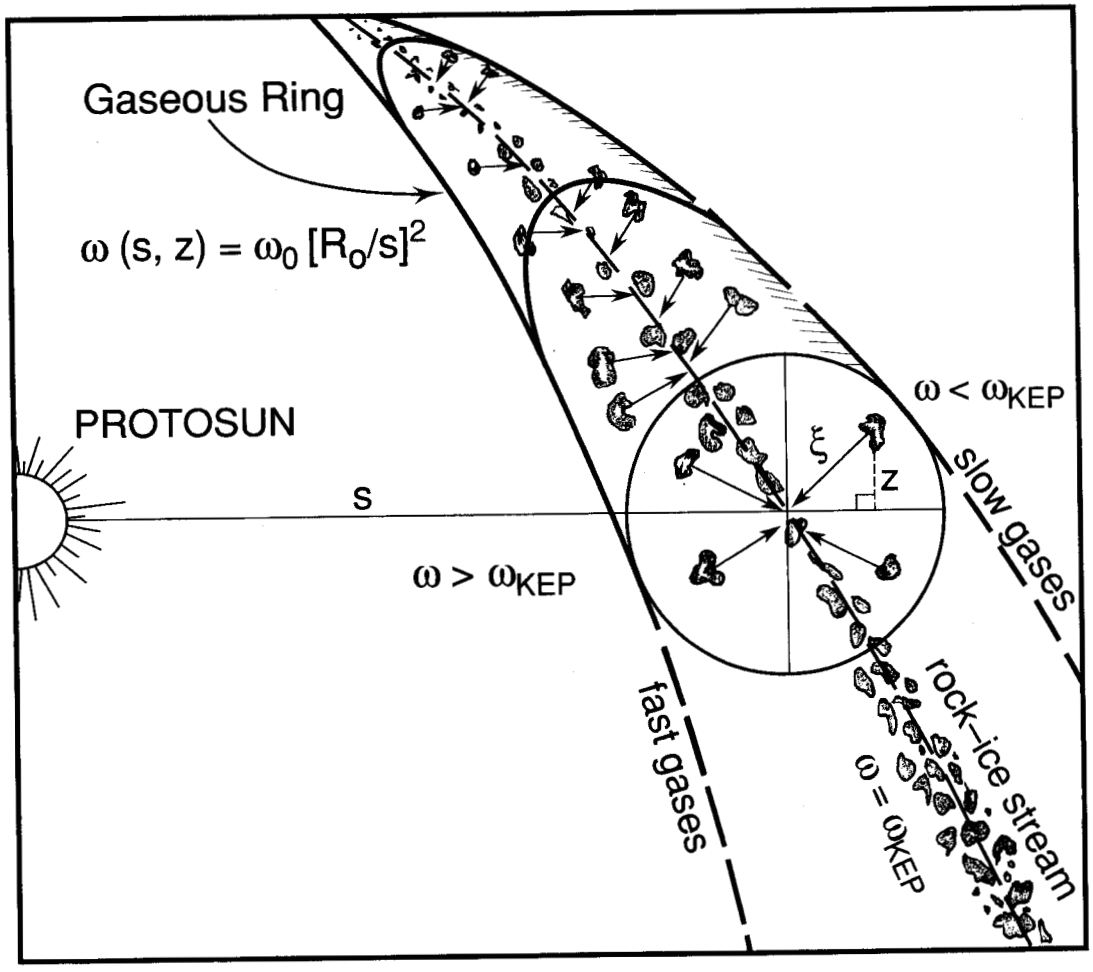

Figure 2

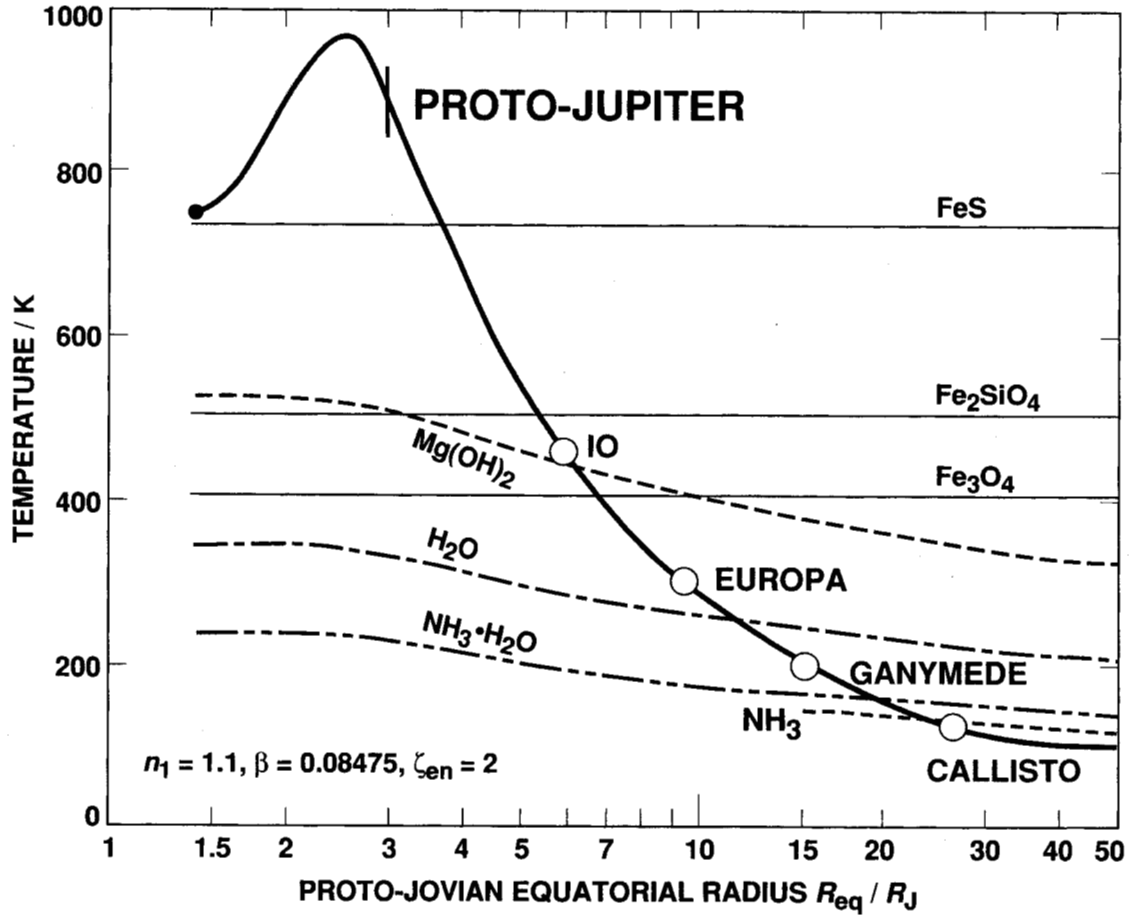

Figure 3

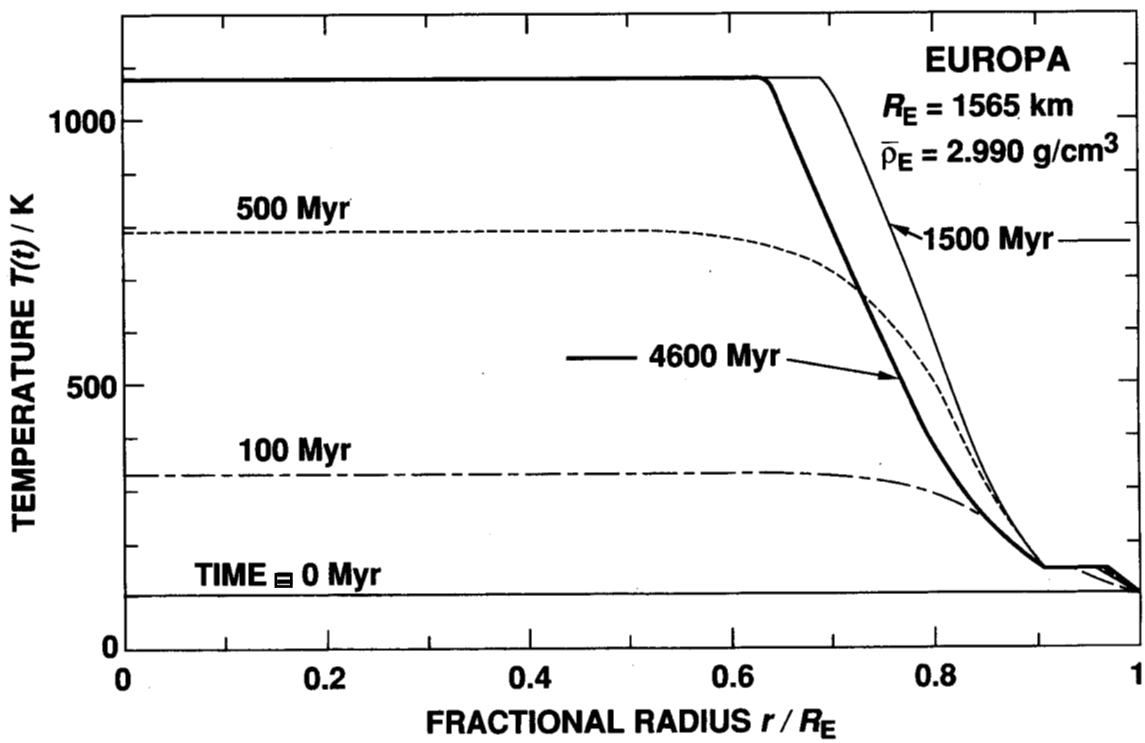

Figure 4

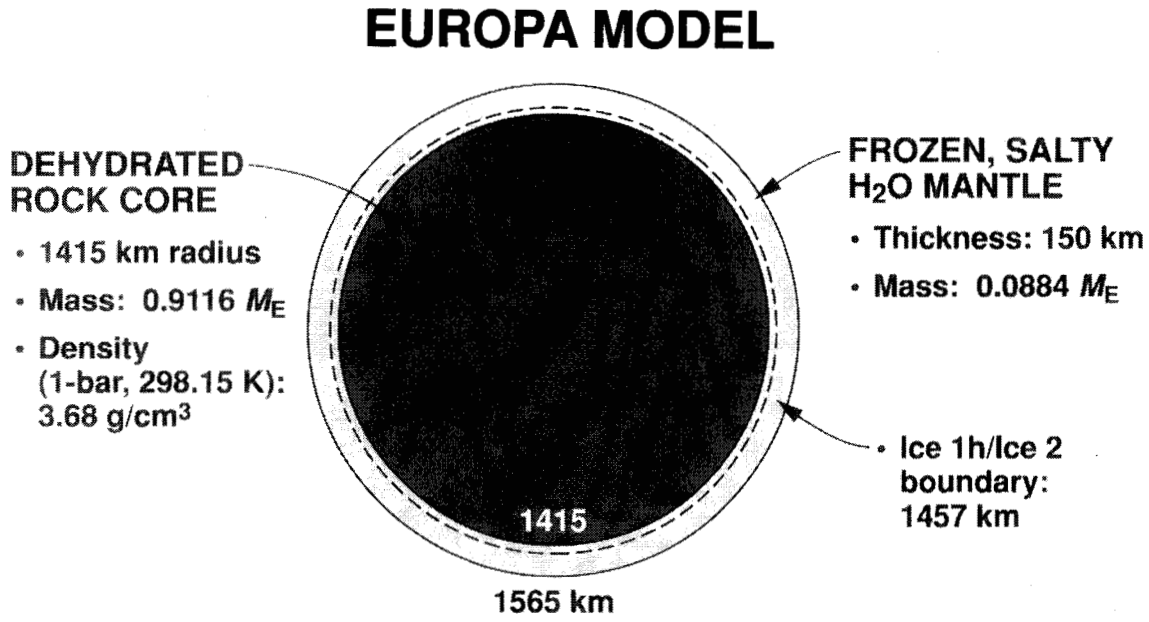

Figure 5

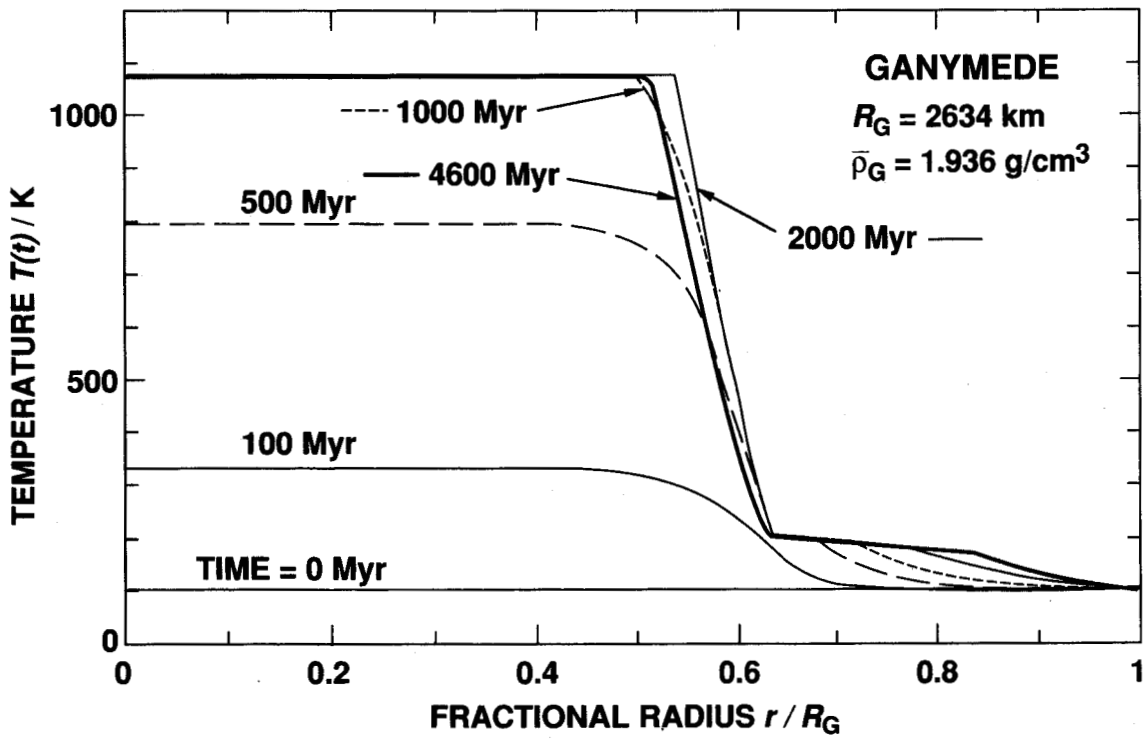

Figure 6

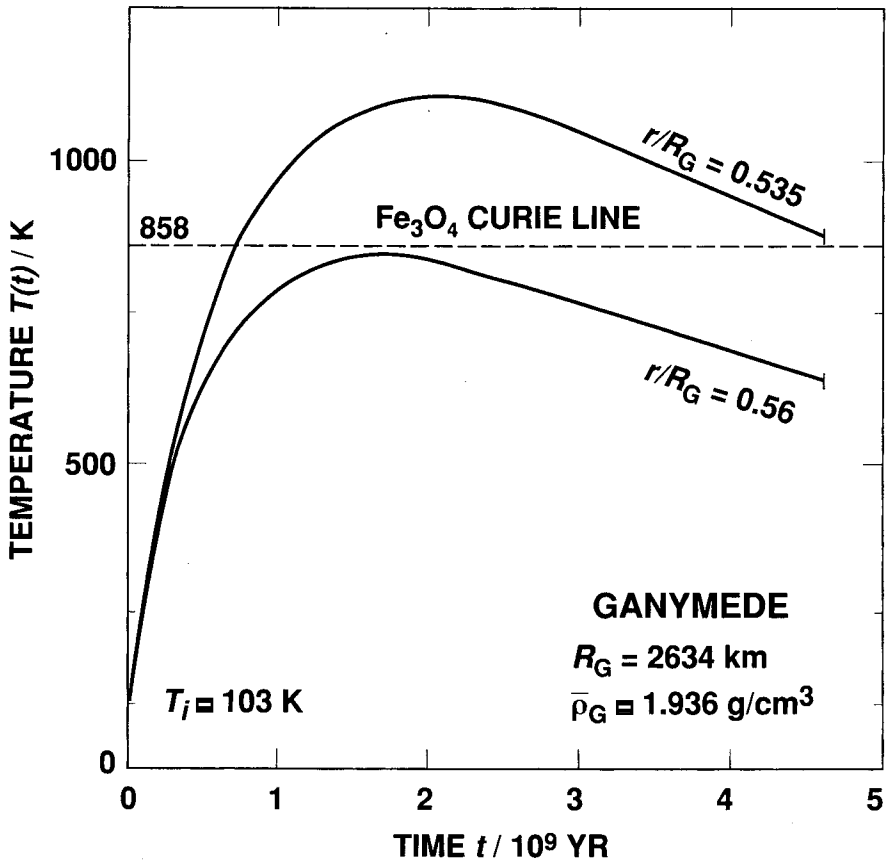

Figure 7

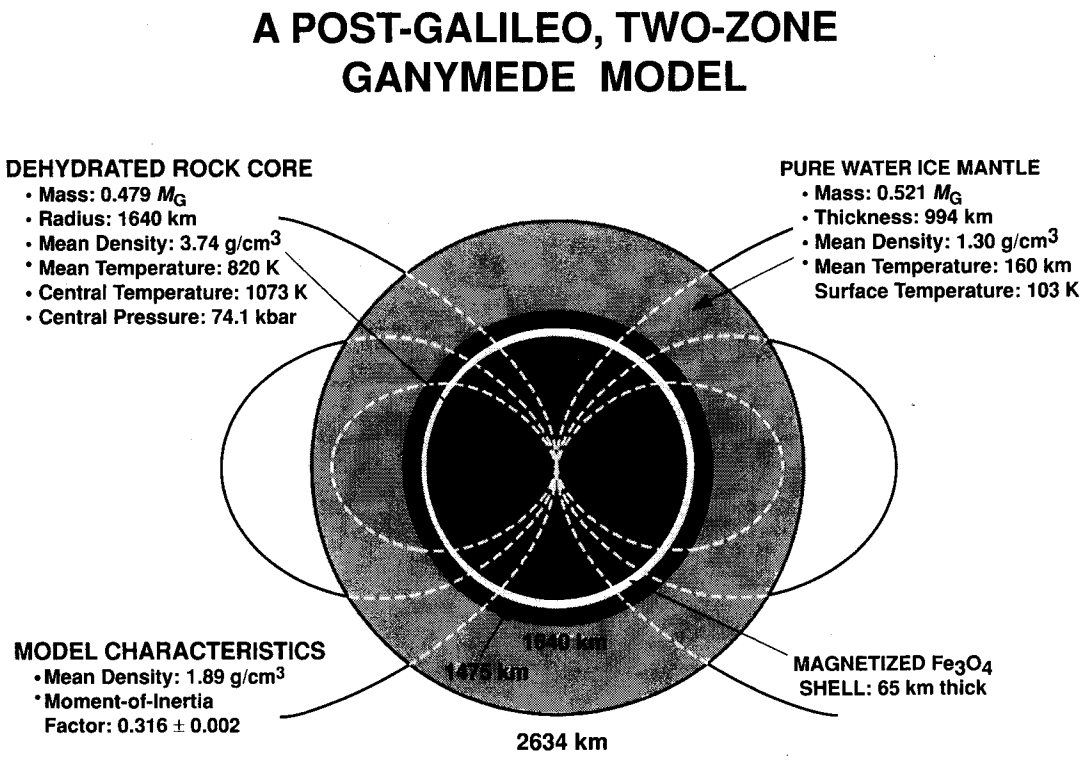

Figure 8

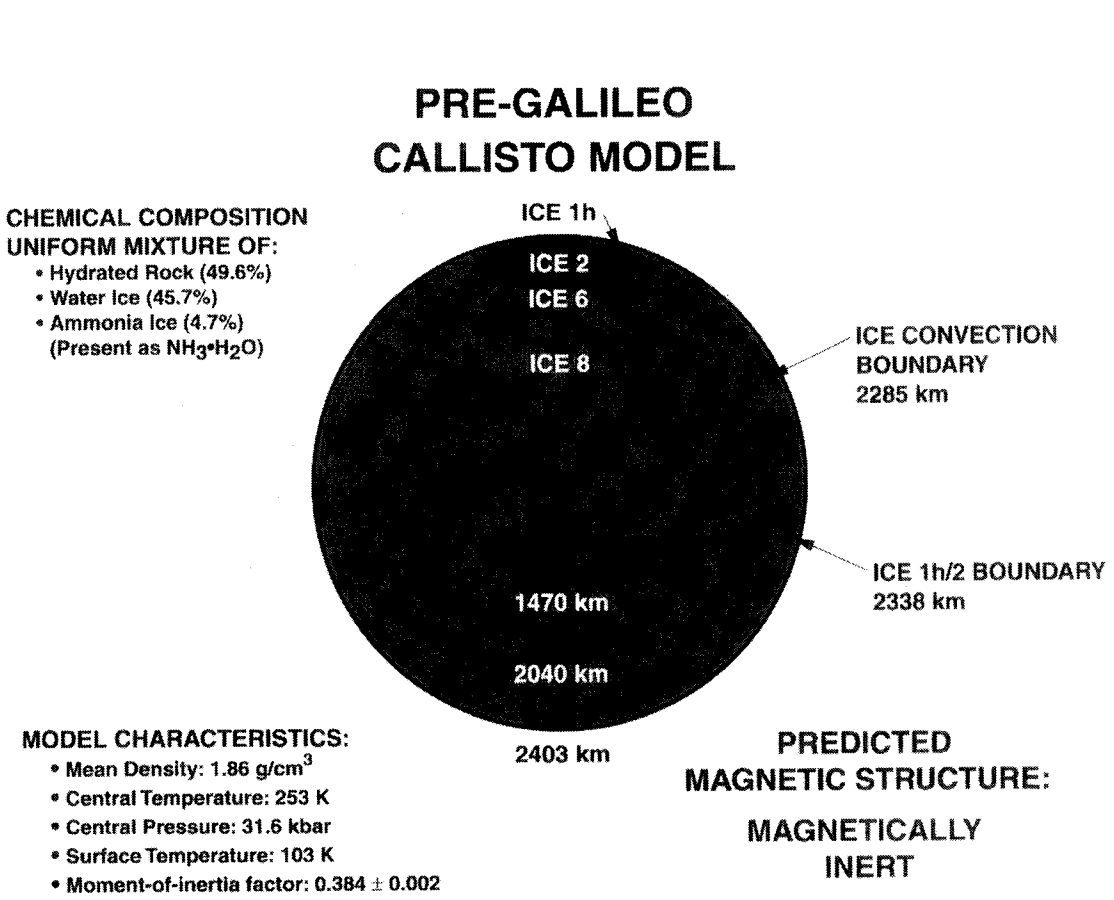

Figure 9

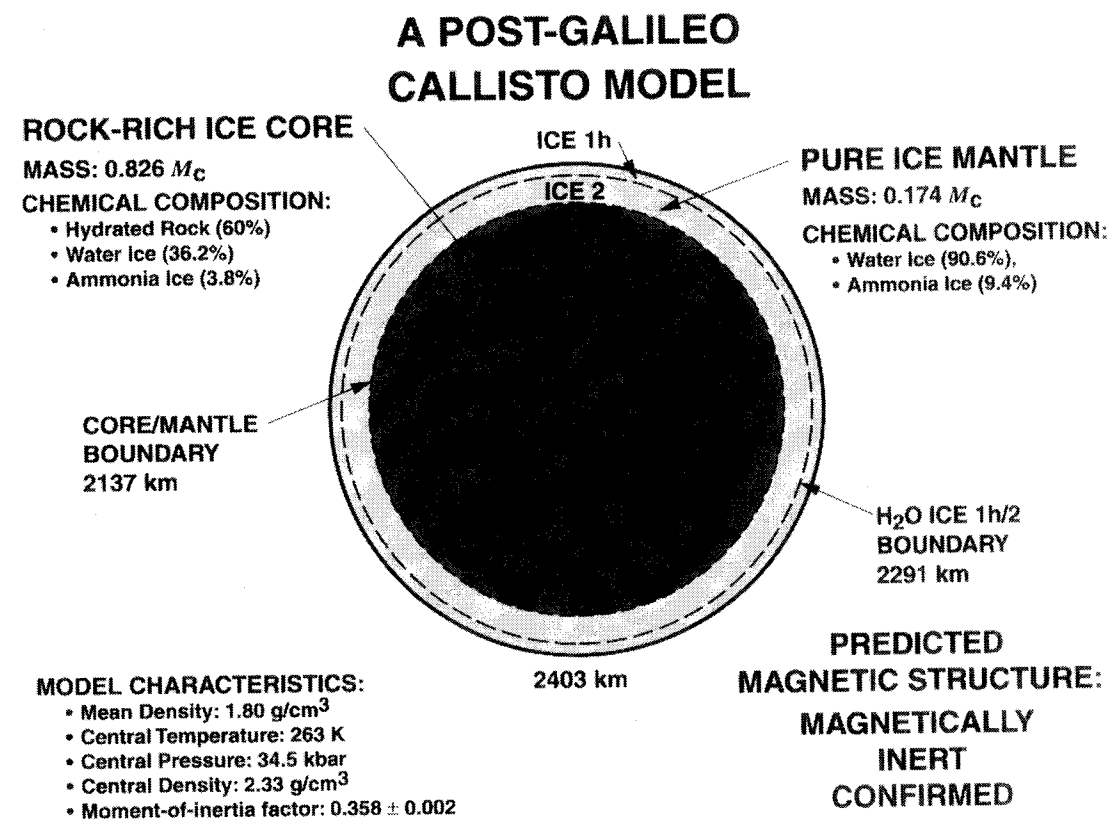

Figure 10